Essential role of hyperacetylated microtubules in innate immunity escape orchestrated by the EBV-encoded BHRF1 protein

Damien Glon[1], Géraldine Vilmen[1, 2†], Daniel Perdiz[3†], Eva Hernandez[1], Guillaume Beauclair[1], Vincent Maréchal[2], Christian Poüs[3, 4], Marion Lussignol[1#] and Audrey Esclatine[1#*]

1. Université Paris-Saclay, CEA, CNRS, Institute for Integrative Biology of the Cell (I2BC), 91198, Gif-sur-Yvette, France
2. CRSA, Centre de Recherche Saint-Antoine, UMRS 938, INSERM, Sorbonne Université, 75012 Paris, France
3. INSERM UMR-S 1193, Université Paris-Saclay, 92296 Châtenay-Malabry, France
4. Biochimie-Hormonologie, APHP, Hôpitaux Universitaires Paris-Saclay, Site Antoine Béclère, 92141 Clamart, France

[†] These authors contributed equally to this work.

[#] These authors share senior authorship.

* For correspondence: audrey.esclatine@universite-paris-saclay.fr (AE)

Competing interests: The authors declare that no competing interests exist.

Abstract

Innate immunity constitutes the first line of defense against viruses, in which mitochondria play an important role in the induction of the interferon (IFN) response. BHRF1, a multifunctional viral protein expressed during Epstein-Barr virus reactivation, modulates mitochondrial dynamics and disrupts the IFN signaling pathway. Mitochondria are mobile organelles that move through the cytoplasm thanks to the cytoskeleton and in particular the microtubule (MT) network. MTs undergo various post-translational modifications, among them tubulin acetylation. In this study, we demonstrated that BHRF1 induces MT hyperacetylation to escape innate immunity. Indeed, expression of BHRF1 induces the aggregation of shortened mitochondria next to the nucleus. This mito-aggresome is organized around the centrosome and its formation is MT-dependent. We also observed that the BHRF1-induced hyperacetylation of MTs involves the α-tubulin acetyltransferase ATAT1. Thanks to a non-acetylatable α-tubulin mutant, we demonstrated that this hyperacetylation is necessary for the mito-aggresome formation. We investigated the mechanism leading to the clustering of mitochondria, and we identified dyneins as motors that are required for the mitochondrial aggregation. Finally, we demonstrated that BHRF1 needs MT hyperacetylation to block the induction of the IFN response. Indeed, in the absence of MT hyperacetylation, BHRF1 is unable to initiate the sequestration of mitochondria into autophagosomes, and mitophagy, which is essential to inhibiting the signaling pathway. Therefore, our results reveal the role of the MT network, and its acetylation level, in the induction of a pro-viral mitophagy.

Introduction

The innate immunity system provides the first line of defense against different invading pathogens. This process is based on the sensing of motifs from the foreign organism, called the pathogen-associated molecular pattern (PAMP), by different host pattern recognition receptors (PRR). In the case of a viral infection, their recognitions notably lead to the induction of the interferon (IFN) response, which leads to the expression of interferon-stimulated genes and the synthesis of cytokines known for their antiviral properties (Lee and Ashkar, 2018).

Mitochondria carry out a crucial role in many cellular processes ranging from energy production to programmed cell death, from calcium homeostasis to cell immunity. They constitute a platform for signaling pathways involved in innate immunity thanks to the MAVS (mitochondrial antiviral signaling protein) receptor, predominantly localized at the mitochondrial outer membrane surface (Arnoult *et al.*, 2011; West *et al.*, 2011). The functions of mitochondria depend on their morphology, which is in turn dependent upon mitochondrial dynamics (including fission, fusion, and motility). Indeed, mitochondria are dynamic organelles that continually switch between cycles of fusion and fission to regulate the network structure (Giacomello *et al.*, 2020). Fission occurs at mitochondria-endoplasmic reticulum (ER) contact sites, which facilitate the recruitment of Drp1 (dynamin related protein 1), which multimerizes and in turn triggers the severing of mitochondria (Pagliuso *et al.*, 2018). Fusion is regulated by both MFN1/2 (mitofusins 1 and 2) and OPA1 (optic atrophy type 1) located at the outer and inner mitochondrial membrane, respectively. Moreover, mitochondria are motile because they are actively recruited to specific cellular locations to respond to their functions. In eukaryotic cells, the cytoskeleton and notably microtubules (MTs) play a critical role in the distribution of mitochondria throughout the cytoplasm by facilitating their transport to areas with high metabolic demands (Frederick and Shaw, 2007; Kruppa and Buss, 2021).

The MT cytoskeleton is a highly dynamic polymer of α and β-tubulin heterodimers, which is involved in a variety of cellular functions, such as supporting cell structures, maintaining cell polarity, but also allowing the transport of organelles. Moreover, it has been shown that the MT network of viral infected cells could be used for intracellular transport of viral particle/genomic material to the sites of replication or assembly (Zheng *et al.*, 2017). A broad range of MT-associated proteins (MAPs) contribute to regulate MT dynamic behavior. MAPs include kinesins and dyneins, which both allow the positioning of organelles and the long-distance transport of vesicles along MT tracks. Kinesins generally transport their cargos toward the plus-end of MTs at the cell periphery. Conversely, dyneins transport their cargos to the minus-end of MTs in the cell center (Hancock, 2014). The relationship between MTs and mitochondrial transport is not completely understood. Mitochondrial movement involves

74 mitochondrial adaptors such as small mitochondrial Rho GTPases Miro1/2 and TRAK1/2 (López-
75 Doménech *et al.*, 2018). Indeed, Miro proteins can engage both kinesin and dynein to mediate the
76 bidirectional movement of mitochondria along MT tracts (Fransson *et al.*, 2006; Frederick and Shaw,
77 2007; Tang, 2018).

78 MT functions are regulated by numerous post-translational modifications such as acetylation,
79 detyrosination, phosphorylation, methylation or polyglutamylation (Janke and Magiera, 2020). Among
80 them the acetylation of α-tubulin, which mainly occurs on the Lysine in position 40 (K40), has emerged
81 as an important regulator of numerous cell functions (Perdiz *et al.*, 2011). For example, α-tubulin
82 acetylation, which is often linked to MT stabilization, may modulate the binding of MAPs (Dompierre
83 *et al.*, 2007; Mackeh *et al.*, 2014; Reed *et al.*, 2006) and therefore may modulate organelle movement.
84 Indeed, stable MTs are particularly involved in mitochondrial transport (Friedman *et al.*, 2010), and it
85 has been reported that acetylation of α-tubulin mediates dynein-dependent transport of mitochondria
86 along MTs (Misawa *et al.*, 2013).

87 In this work, we aimed at studying the role of the MT network in the innate immunity escape induced
88 by the Epstein-Barr virus (EBV). BHRF1 is a viral Bcl-2 homolog (Khanim *et al.*, 1997), and our group
89 recently unravelled its novel functions in innate immunity, related to its mitochondrial localization
90 (Vilmen *et al.*, 2020). We demonstrated that BHRF1 disturbs mitochondrial dynamics and subsequently
91 stimulates autophagy. More precisely, BHRF1 induces mitophagy, a cellular process that can
92 specifically sequester and degrade mitochondria by autophagy, and we have shown that BHRF1-
93 induced mitophagy participates in the inhibition of type I IFN response by EBV (Vilmen *et al.*, 2020).
94 Here, we described the importance of the MT hyperacetylation on the mitochondrial clustering and,
95 more unexpectedly, on the capability of BHRF1 to counteract the IFN induction.

96 ## Results

97 ### BHRF1-induced mito-aggresomes are organized around the centrosomes

98 The EBV-encoded BHRF1 localizes to mitochondria, and its expression in HeLa cells dramatically alters
99 mitochondrial dynamics and distribution, (Vilmen *et al.*, 2020). By confocal microscopy, we observed
100 abnormal mitochondrial aggregates close to the nucleus in BHRF1-expressing cells, whereas in control
101 cells (empty vector [EV] transfection), mitochondria remained distributed throughout the cytoplasm
102 (***Figure 1A***). This mitochondrial phenotype, known as mito-aggresome, is in accordance with our
103 previous observations. We arbitrarily consider that, when the compaction index (CI) of mitochondria
104 is above 0.4, the cell presents a mito-aggresome, whereas when the CI value is below 0.4, mitochondria
105 are distributed homogeneously throughout the cell cytoplasm (Narendra *et al.*, 2010; Vilmen *et al.*,
106 2020). The expression of BHRF1 significantly increased the CI values, which corresponds to the
107 formation of a mito-aggresome in almost 80% of the cells (***Figure 1B***). Since BHRF1 is associated with
108 mitochondrial fragmentation (***Figure 1A - insets***), we precisely evaluated mitochondrial shape by
109 calculation of the aspect ratio (AR) and the form factor (FF), two parameters which reflect the
110 mitochondrial length and the branching of mitochondria, respectively. As calculated in ***Figure 1C***,
111 BHRF1 expression significantly reduced both AR and FF parameters, confirming an induction of
112 mitochondrial fission.

113 As mitochondria localize near the nucleus, the involvement of the MT network in this mitochondrial
114 redistribution was investigated. In mammalian cells, mitochondria move along cytoskeletal tracks to
115 sites of high-energy demand in an MT-dependent manner (Detmer and Chan, 2007). At interphase, the
116 MT network radiates from the centrosome, the main MT organizing center for directing the polarity
117 and the orientation of MTs. By co-staining BHRF1-expressing cells for mitochondria and pericentrin, a
118 classical centrosomal marker, we observed that mitochondria are concentrated around the
119 centrosome to form a mito-aggresome (***Figure 1D***). Moreover, a 3D reconstruction confirmed the
120 clustering of BHRF1 in the vicinity of the nucleus around the centrosome (***Supplementary file 1***).

121 ### The MT network is required for BHRF1-induced mito-aggresome formation

122 To test whether MTs play a role in the mitochondrial redistribution following BHRF1 expression, the
123 whole MT network was disassembled using a treatment mixing nocodazole, a classical MT-destabilizing
124 drug, and exposure to cold (Geeraert *et al.*, 2010). As shown in ***Figure 1E - left panel*** this treatment
125 disassembled MTs (fuzzy staining of α-tubulin). The removal of nocodazole followed by 1 hour in a
126 warm complete medium at 37°C restored the MT network (***Figure 1E - right panel***). In cells without
127 BHRF1 expression, mitochondria were homogeneously distributed in the cytoplasm, and the
128 disorganization of the MT network had no impact on their distribution. Conversely, mitochondrial

129 aggregation in BHRF1-expressing cells was abolished when MTs were depolymerized (***Figure 1E - left***
130 ***panel***) and mitochondria were then distributed throughout the cell (CI values mainly below 0.4). This
131 phenomenon was reversible since the mitochondria rapidly re-aggregated to different extents within
132 1 hour after reassembly of the MT network (most of the CI values above 0.4) (***Figure 1E - right panel***).
133 In contrast, mitochondria in non-transfected neighboring cells remained scattered within the
134 cytoplasm after nocodazole removal. The quantification of mito-aggresomes in BHRF1-positive cells
135 showed that whereas less than 20% of the cells presented mitochondrial aggregation after
136 depolymerization treatment (***Figure 1F***), this proportion went back to more than 50% after
137 repolymerization of the MTs (compare to 80% without treatment). We concluded that the MT network
138 is required for the mito-aggresome formation.

139 As the actin network is also known to be involved in mitochondrial transport and fission (De Vos *et al.*,
140 2005; López-Doménech *et al.*, 2018), we also checked if F-actin disorganization affects the
141 mitochondrial phenotype induced by BHRF1. In order to do so, we treated HeLa cells with cytochalasin
142 B to disrupt F-actin but we did not observe any changes in the mitochondrial phenotype in BHRF1-
143 positive cells (***Supplementary file 2A***). BHRF1 still induced the mitochondrial aggregation and fission
144 at the same level as in the control (***Supplementary file 2B and C***). Therefore, the actin network does
145 not seem to be involved in the mitochondrial phenotype.

146 **BHRF1 induces MT hyperacetylation, which is required for the mito-aggresome formation**

147 We next explored whether BHRF1 could modify the MT network by assessing its acetylation level. Upon
148 BHRF1 expression, whereas α-tubulin staining was unchanged, acetyl-α-tubulin was redistributed and
149 colocalized with BHRF1 (***Figure 2A***). Moreover, we observed a brighter signal of acetyl-α-tubulin,
150 suggesting an increase in α-tubulin acetylation. This was confirmed by western-blot analysis, showing
151 an increase of 60% under BHRF1 expression (***Figure 2B***).

152 To determine whether this hyperacetylation could be involved in BHRF1-induced mitochondrial
153 alterations, we expressed a non-acetylatable α-tubulin mutant (mCherry-α-tubulin K40A) which
154 prevents MT hyperacetylation (Dompierre *et al.*, 2007). It has previously been reported that this non-
155 acetylatable α-tubulin mutant does not alter the MT network and is present in the entire MT network
156 (Geeraert *et al.*, 2010). Notably, when α-tubulin K40A is expressed, endogenous α-tubulin still remains
157 acetylatable. However, the MT network's ability to be hyperacetylated is prevented, since α-tubulin
158 acetylation only occurs on protofilaments and the MT network is totally decorated with this non-
159 acetylatable α-tubulin. We thus verified by immunoblot analysis that BHRF1 was unable to induce
160 hyperacetylation of α-tubulin when the mutant α-tubulin K40A was expressed (***Figure 2C***). Then, the
161 impact of α-tubulin K40A on the clustering of mitochondria was analyzed (***Figures 2D and E***). In cells

162 co-expressing α-tubulin K40A and BHRF1, CI mean value was below 0.4 and mitochondria were
163 homogeneously distributed throughout the cytoplasm, similarly to control cells. Thus, we concluded
164 that BHRF1-induced mito-aggresome formation depends on MT hyperacetylation.

165 Interestingly, we observed that without α-tubulin hyperacetylation, BHRF1 was still able to promote
166 mitochondrial fragmentation (**Figure 2F**). Confocal images (***Figure 2D, insets***) clearly showed that upon
167 BHRF1 expression (for both WT and K40A conditions) mitochondria were drastically smaller. Therefore,
168 hyperacetylation of MTs is essential for BHRF1-induced mito-aggresome formation but not for
169 mitochondrial fission.

170 **MT hyperacetylation is necessary to the inhibition of type I IFN response by BHRF1**

171 Mitochondria appear to be central organelles for the induction of antiviral innate immunity. RIG-I
172 (retinoic acid-inducible gene) and MDA5 (melanoma differentiation-associated protein 5) are two
173 cytoplasmic PRRs that detect viral genome. Upon activation, these receptors are translocated to the
174 mitochondria to interact with the mitochondrial-resident protein MAVS that recruits and activates
175 TBK1 (TANK-binding kinase 1). This kinase is required for the phosphorylation of the transcription
176 factors IRF3 and IRF7 (interferon regulatory factors 3 and 7), leading to their dimerization, nuclear
177 translocation and the subsequent activation of type I IFN promoter (Arnoult *et al.*, 2011; West *et al.*,
178 2011). Our group and others previously demonstrated that impairing the mitochondrial
179 morphodynamics leads to the inhibition of IFN response (Castanier *et al.*, 2010; Chatel-Chaix *et al.*,
180 2016; Vilmen *et al.*, 2020; Yoshizumi *et al.*, 2014). Considering the importance of tubulin
181 hyperacetylation for the formation of mito-aggresomes, we sought to know whether MT
182 hyperacetylation was required for the inhibition of type I IFN response by BHRF1. We performed an
183 IFN-β promoter-driven luciferase reporter assay in BHRF1-expressing HEK293T cells (***Figure 3A***). To
184 activate the IFN-signaling pathway, we expressed an active form of RIG-I, designated ΔRIG-I (2xCARD)
185 (Yoneyama *et al.*, 2004), which constitutively activates MAVS-dependent pathway through CARD
186 domains interaction. As previously observed, BHRF1 dramatically blocked the IFN-β promoter
187 activation, however, the expression of the α-tubulin K40A significantly prevented this inhibition (***Figure***
188 ***3A***). To confirm our results, we examined the cellular localization of IRF3 by immunofluorescence. In
189 basal conditions, IRF3 staining is diffuse throughout the cytoplasm. When ΔRIG-I (2xCARD) is
190 expressed, IRF3 translocates from the cytoplasm into the nucleus but expression of BHRF1 blocked this
191 translocation (***Figure 3B***). However, when MT hyperacetylation was prevented, BHRF1 was not able to
192 block IRF3 nuclear translocation (***Figure 3B***). Quantification of this assay showed that expression of the
193 non-acetylatable form of α-tubulin totally restored IRF3 nuclear translocation upon BHRF1 expression
194 (***Figure 3C***). Therefore, our results demonstrated that MT hyperacetylation is required for BHRF1 to
195 inhibit type I IFN response.

196 **BHRF1 requires acetyltransferase ATAT1 to modify MTs and form mito-aggresomes.**

197 Thereafter, we wanted to characterize the mechanism of MT hyperacetylation induction by BHRF1.
198 Tubulin acetylation results from the balance between the activities of tubulin acetyltransferases and
199 deacetylases. Therefore, a hyperacetylation of the MTs can be the consequence of either the inhibition
200 of deacetylases or the activation of an acetyltransferase. First of all, we wanted to investigate a
201 potential inhibitory role of BHRF1 on the two main α-tubulin deacetylases, HDAC6 (histone deacetylase
202 6) and SIRT2 (sirtuin type 2) (Hubbert *et al.*, 2002; North *et al.*, 2003). Indeed, it has been observed
203 that knockdown of SIRT2 results in an aberrant mitochondrial distribution in the perinuclear region
204 (Misawa *et al.*, 2013), and another study showed that the depletion of SIRT2 results in nuclear
205 envelope shape defects (Kaufmann *et al.*, 2016). These observations are clearly similar to the effect of
206 BHRF1 on mitochondria, as well as its distribution around the nuclear envelope and the modification
207 of the nucleus shape (***Figure 1A***). Thus, we performed an *in vitro* tubulin deacetylation assay (Mackeh
208 *et al.*, 2014). This test consists of mixing the highly acetylated porcine brain tubulin with lysates of
209 BHRF1-expressing cells. Lysate of control EV-transfected cells reduces the acetylation of tubulin by
210 approximately 50% compared to condition without cell lysate (***Figure 4A***). The same deacetylase
211 activity is observed with BHRF1-positive lysates, indicating that BHRF1 does not inhibit the
212 deacetylases.

213 We subsequently investigated the role of ATAT1 (alpha-tubulin N-acetyltransferase 1) (Shida *et al.*,
214 2010). We knocked down ATAT1 expression by a siRNA approach and observed no more detectable
215 acetylation activity under BHRF1 expression (***Figure 4B***), indicating involvement of ATAT1 in BHRF1-
216 induced hyperacetylation. Then, we checked the mitochondrial network and observed that the
217 knockdown of ATAT1 prevents the mito-aggresome formation but not mitochondrial fission (***Figure***
218 ***4C-E***). These results led us to conclude that BHRF1 activates the acetyltransferase ATAT1, leading to
219 MT hyperacetylation and subsequent mito-aggresome formation.

220 **Mito-aggresome formation requires retrograde transport of mitochondria via dyneins**

221 As observed in ***Figure 1E***, after removal of nocodazole and regrowth of the MT network, mitochondria
222 rapidly re-aggregated in BHRF1-expressing cells, indicating that an MT-dependent motor activity is
223 involved in the mito-aggresome formation. Moreover, the hyperacetylation of MTs has been
224 previously shown to facilitate the recruitment and binding of MAPs on the tubulin (Dompierre *et al.*,
225 2007). We therefore hypothesized that BHRF1-induced mitochondrial aggregation next to the nucleus
226 could use dyneins. To investigate this hypothesis, we inhibited dynein functions by overexpression of
227 p50-dynamitin. The overexpression of one subunit of the dynactin complex (p50-dynamitin) disrupts
228 it and results in the dissociation of dyneins from the MT network. We observed that the expression of

229 this construction totally prevents mitochondrial aggregation in BHRF1-expressing cells (***Figures 5A and***
230 ***5B***). Moreover, the ability of BHRF1 to induce mitochondrial fission was decreased when dyneins were
231 inhibited, as we observed a partial but significant restoration of mitochondrial fission parameters (AR
232 and FF; ***Figure 5C***).

233 To confirm the importance of dynein motors in the mito-aggresome formation, we treated cells with
234 ciliobrevin-D, a specific inhibitor of dyneins, which blocks their gliding along MTs and their ATPase
235 activity. As with overexpression of p50-dynamitin, BHRF1 was not able to induce mito-aggresomes in
236 cells treated with ciliobrevin-D (***Supplementary file 4B and 4C***). However, BHRF1 still induced a slight
237 mitochondrial fission phenomenon (***Supplementary file 4B and 4D***). Altogether, these results
238 demonstrate that fragmented mitochondria are aggregated next to the nucleus in a dynein-dependent
239 manner.

240 **MT hyperacetylation does not affect BHRF1-pro-autophagic activity, but is required for the**
241 **first step of mitophagy induction**

242 Our group previously demonstrated that BHRF1 first stimulates autophagy and then induces
243 mitophagy, the selective removal of mitochondria (Vilmen *et al.*, 2020). Autophagy is a conserved
244 cellular process allowing the removal and recycling of damaged or supernumerary cellular
245 components. This process involves double-membrane vesicles, called autophagosomes, which fuse
246 with lysosomes to degrade the content. Selective autophagy consists of the recognition of a specific
247 cargo by a molecular receptor that links the cargo to the autophagosome for its removal (Green and
248 Levine, 2014).

249 Several studies demonstrated the role of MTs during the autophagic process, notably during the
250 formation of the autophagosomes (Geeraert *et al.*, 2010; Köchl *et al.*, 2006; Mackeh *et al.*, 2013). Thus,
251 we investigated whether BHRF1 could stimulate autophagy dependent on MT hyperacetylation. The
252 autophagic flux was studied in HeLa cells co-expressing α-tubulin K40A and BHRF1. We first analyzed
253 by immunofluorescence the accumulation of LC3 (microtubule associated protein 1 light chain 3), a
254 classical marker of autophagosomes in the presence or absence of chloroquine (CQ), an inhibitor of
255 the autophagic flux. When non-acetylatable α-tubulin was expressed, BHRF1 induced a clear
256 accumulation of LC3 dots in the cytoplasm, and even more after CQ treatment (***Figure 6A***). We
257 quantified LC3 dots and we observed no difference when MTs were hyperacetylated or not (***Figure 6B***
258 ***and supplementary file 5A***). We confirmed the result by analyzing the accumulation of lipidated LC3
259 (LC3-II) by immunoblot and we observed an increase in LC3-II levels in BHRF1-expressing cells,
260 independently of MT hyperacetylation (***Figure 6C and Supplementary file 5B***). This increase is

261 potentiated after CQ treatment. Therefore, we concluded that BHRF1 stimulates the biogenesis of
262 autophagosomes and the autophagic flux independently of MT hyperacetylation.

263 Mitochondrial aggregation in the perinuclear region has been already documented as essential to the
264 efficient removal of mitochondria by mitophagy (Lee *et al.*, 2010). Although autophagy stimulation
265 occurs independently of MT hyperacetylation, we investigated whether BHRF1-induced mitophagy
266 depends on tubulin hyperacetylation by evaluating the colocalization between mitochondria and
267 autophagosomes in cells co-expressing α-tubulin K40A and BHRF1. When MT hyperacetylation was
268 prevented, mitochondria did not colocalize anymore with autophagosomes (***Figure 6D***). The
269 quantification of colocalization intensity, measured by Manders' coefficient, confirmed that
270 mitochondrial sequestration in autophagic vesicles did not occur when the mito-aggresome formation
271 was impeded (***Figure 6E***).
272 We then decided to investigate whether, conversely, autophagy was involved in BHRF1-induced MT
273 hyperacetylation. We observed that inhibition of autophagy by treatment with 3-methyladenine (3-
274 MA) or spautin-1 impeded the MT hyperacetylation (***Supplementary file 5C***).

275 Altogether, these results demonstrated that MT hyperacetylation was essential for the mitochondrial
276 sequestration but not for the induction of autophagy. In fact, BHRF1 needs autophagy activation to
277 induce MT hyperacetylation. Therefore, we uncovered a novel mechanism to counteract anti-viral
278 immunity, involving the initiation of mitophagy through the induction of tubulin hyperacetylation by
279 BHRF1.
280

281 ## Discussion

282 We previously demonstrated that EBV-encoded BHRF1 blocks the IFN response by modifying the
283 mitochondrial dynamics and by stimulating autophagy (Vilmen *et al.*, 2020). Expression of this viral
284 protein induces mitochondrial fission, followed by the relocalization of fragmented mitochondria close
285 to the nucleus in the proximity of the centrosome (***Figure 1 and Supplementary file 1***). Mitochondria
286 are usually driven over long distances along MTs by motor proteins, thanks to the Miro/TRAK adaptor
287 complex (Kruppa and Buss, 2021). Here, we demonstrate that the MT network is hijacked by BHRF1 to
288 ensure the mito-aggresome formation and to consequently block the antiviral innate immunity
289 (***Figures 1 and 3***). We notably observed that disruption of the MT network impedes mitochondrial
290 trafficking to the centrosome, suggesting a dynamic process. In accordance, our results indicate that
291 BHRF1 requires the MT-based motor dynein, that typically move towards the minus-end of MT, to
292 regroup mitochondria in the perinuclear region (***Figure 5 and Supplementary file 4***).

293 The cytoplasmic dynein complex contains a pair of identical heavy chains which comprises the MT-
294 binding domain. Each heavy chain harbors a motor domain that belongs to the AAA+ superfamily.
295 Additional subunits complete this complex, each of which functions as a dimer; these are the
296 intermediate chain, light-intermediate chain and three types of light chain (TCTEX, DYNLL1 and
297 Roadblock) (Janke and Magiera, 2020; Roberts *et al.*, 2013). It has been reported that DYNLL1 can
298 interact with BCL2L11/BIM, a proapoptotic BH3-only protein expressed at the mitochondrial outer
299 membrane, and can regulate its proapoptotic activity (Puthalakath *et al.*, 1999; Singh *et al.*, 2019).
300 Interestingly, it has been shown that BIM binds to BECN1, a key regulator of autophagosome
301 formation, linking BECN1 to DYNLL1 and MTs, and leading to autophagy inhibition (Luo *et al.*, 2012).
302 We and others demonstrated that BHRF1 can stimulate autophagy through its interaction with BECN1
303 and block apoptosis through its interaction with BIM (Desbien *et al.*, 2009; Kvansakul *et al.*, 2010;
304 Vilmen *et al.*, 2020). Therefore, we hypothesize that BIM could connect mitochondria to MTs by
305 interacting with BHRF1 and the MT-trafficking apparatus. The formation of this complex could explain
306 the mitochondrial movement toward the centrosome and participate in autophagy regulation.

307 In eukaryotic cells, MTs are generally built from 13 chains of α-β tubulin dimers known as
308 protofilaments. Properties and behaviors of MTs can be modulated by numerous post-translational
309 modifications on both α and β tubulin (Janke and Magiera, 2020; Janke and Montagnac, 2017). We
310 observed that the expression of BHRF1 increases the acetylation of α-tubulin on the lysine in position
311 40 (K40) and that acetylated MTs are required for the mito-aggresome formation (***Figure 2***).
312 Acetylation of α-tubulin subtly changes its structure and disrupts the interaction between adjacent α-
313 tubulins of neighboring protofilaments (Eshun-Wilson *et al.*, 2019). The loss of this connection weakens

interactions between protofilaments, which facilitates their sliding and decreases the flexural rigidity of MTs, making them more resistant to mechanical bending-induced breakage and disassembly (Portran *et al.*, 2017).

The hyperacetylation of MTs can result from either activation of tubulin acetyltransferases or inhibition of deacetylases (Li and Yang, 2015). Knockdown of the acetyltransferase ATAT1 by siRNA impedes the acetylation of α-tubulin and the mito-aggresome formation upon BHRF1 expression (***Figure 4***). Therefore, our results demonstrate that BHRF1 induces MT hyperacetylation by activating ATAT1. The expression of the non-acetylatable K40A mutant form of tubulin confirmed that tubulin acetylation, and not just ATAT1 activity, is required for the mito-aggresome formation and sequestration of mitochondria in autophagosomes (***Figures 2 and 6***). We also investigated a potential inhibitory role of BHRF1 on tubulin deacetylases. However, our results showed that BHRF1 does not impact the global tubulin deacetylase activity of BHRF1-expressing cells, suggesting that activities of HDAC6 and SIRT2, the two main α-tubulin deacetylases, are not inhibited by BHRF1 (Hubbert *et al.*, 2002; North *et al.*, 2003).

Hyperacetylation of MTs in the presence of BHRF1 could directly allow the spatial arrangement of mitochondria to the centrosome but the precise role of acetylated MTs will need to be further investigated. Misawa *et al.* demonstrated that accumulation of acetylated α-tubulin by knockdown of SIRT2 results in an aberrant mitochondrial distribution in the perinuclear region (Misawa *et al.*, 2013), similar to what was observed with BHRF1. Moreover, acetylated α-tubulin is more abundant in stable MTs, which are particularly implicated in mitochondrial transport (Friedman *et al.*, 2010). Interestingly, it has been shown that MT hyperacetylation *in vitro* and in cells causes the recruitment of dynein and kinesin-1 to MTs, which notably stimulates anterograde and retrograde transport of organelles in neurons or epithelial cells (Dompierre *et al.*, 2007; Geeraert *et al.*, 2010). BHRF1-induced acetylation of α-tubulin could thus increase dynein recruitment to MTs, facilitating the traffic of fragmented mitochondria to the centrosome.

It is interesting to note that MT hyperacetylation induced by BHRF1 is not involved in mitochondrial fission, since expression of the non-acetylatable α-tubulin mutant K40A or the knockdown of ATAT1 have no impact on mitochondrial length or branching parameters (***Figure 2F and Figure 4E***). We previously demonstrated that BHRF1 increases mitochondrial fragmentation in a Drp1-dependent manner (Vilmen *et al.*, 2020). Moreover, BHRF1 increases the dephosphorylation of Drp1 in position Ser637, which is then recruited to mitochondria to allow mitochondrial fission (Vilmen *et al.*, 2020). In our context, the lack of direct involvement of acetylated MTs on mitochondrial fission could seem quite surprising, since it has been previously shown that MT hyperacetylation triggered by acute

347 hyperosmotic stress enhanced mitochondrial fission (Perdiz *et al.*, 2017). However, in the context of
348 this acute stress, mitochondrial fission is associated with an increased level of Ser616 phosphorylation
349 of Drp1, a different post-translational modification from the one observed upon BHRF1 expression.
350 Implication of hyperacetylated-MT in the mitochondrial fission process may thus differ according to
351 the type of cellular stress.

352 BHRF1 is a multifunction protein (*e.g.* anti-apoptotic and pro-autophagic) localized at both the ER and
353 the mitochondrial membranes. Since mitochondrial fission occurs at contact sites between ER and
354 mitochondria, ER-localized BHRF1 could be involved in the ER remodeling into tubules which enwrap
355 mitochondria and initiate the constriction of mitochondrial membranes before the recruitment of Drp1
356 (Friedman *et al.*, 2011). Conversely, the impact of BHRF1 on MT acetylation and mitochondrial
357 trafficking could be related to its mitochondrial membrane localization.

358 We observed that MT hyperacetylation is not necessary to induce autophagy upon BHRF1 expression,
359 whereas inhibition of autophagy impedes MT acetylation (***Figure 6 and Supplementary file 5***). This
360 could seem unexpected, since several studies have demonstrated the role of MT acetylation in
361 autophagosome formation and maturation, and the autophagy flux is directly correlated to MT
362 acetylation levels (Esteves *et al.*, 2019; Geeraert *et al.*, 2010; Xie *et al.*, 2010). For example, initiation
363 of starvation-induced autophagy requires MT acetylation to recruit dynein and kinesin-1 and to allow
364 JNK (c-Jun N-terminal kinase) activation, leading to BECN1 release (Geeraert *et al.*, 2010). Very
365 recently, it has been shown that p27, a tumor suppressor which promotes autophagy in response to
366 glucose starvation, stimulates MT acetylation by binding to and stabilizing ATAT1, to allow the delivery
367 of autophagosomes in the proximity of the centrosome for efficient fusion with lysosomes (Nowosad
368 *et al.*, 2021). However, MTs is not involved in autophagosome formation in basal autophagy (Mackeh
369 *et al.*, 2013). Although BHRF1-induced MT hyperacetylation has no role in non-selective autophagy,
370 we observed that it is essential for BHRF1 to induce mitophagy since, in the absence of α-tubulin
371 acetylation, BHRF1 does not induce mitochondrial sequestration into autophagosomes (***Figure 6***). This
372 suggests that formation of the autophagosomal membranes around mitochondria requires acetylated
373 MTs.

374 Numerous strategies are used by viruses to counteract or evade the innate immune response. We
375 describe in this study a novel mechanism of a viral immune escape. Indeed, we report that MT
376 hyperacetylation induced by BHRF1 can block IFN production, via mitophagy stimulation. Several
377 proteins expressed by different viruses, such as human parainfluenza virus type 3, influenza A virus
378 (IAV), or Hantaan virus (HTNV), are known to control type I IFN response by stimulating mitophagy
379 (Ding *et al.*, 2017; Wang *et al.*, 2019, 2020). The viral glycoprotein (Gn) encoded by HTNV translocates

380 to mitochondria, induces complete mitophagy which leads to MAVS degradation and subsequently
381 impairs innate immune response (Wang *et al.*, 2020). PB1-F2 is a non-structural IAV-encoded protein
382 constitutively localized to the mitochondrial inner membrane space (Yoshizumi *et al.*, 2014). At
383 mitochondria, the interaction of PB1-F2 with LC3B and mitochondrial TUFM (Tu translation elongation
384 factor) similarly leads to mitophagy induction, MAVS degradation and restrains type I IFN production
385 (Wang *et al.*, 2020). Whether these pro-viral mechanisms depend on the tubulin acetylation level
386 needs to be explored.

387 The role of MT-dependent mitochondrial movement has been previously described to be involved in
388 the NLRP3 (NOD-like receptor family pyrin domain containing 3) inflammasome, a complex that also
389 contributes to antiviral innate immunity by the secretion of pro-inflammatory cytokines, such as
390 interleukin-1β and 18 (Zhao and Zhao, 2020). Detection of a viral infection or a danger signal can trigger
391 the formation of this inflammasome, which is comprises of NLRP3, the adaptor protein ASC (apoptosis-
392 associated speck-like protein containing a CARD), and the effector protease caspase-1. Mitochondrial
393 dynamics and movement are involved in inflammasome activation, to bring closer the fraction of ASC
394 which resides on the mitochondria to NLRP3, located in the ER under resting conditions. It has been
395 reported that acetylated MTs and dyneins are essential for the relocalization of mitochondria in the
396 perinuclear region and the inflammasome complex formation (Misawa *et al.*, 2013). However, several
397 studies have also reported that the activation of mitophagy can preclude NLRP3 inflammasome
398 formation by preventing the release of mitochondrial DNA and ROS (Mishra *et al.*, 2021; Zhong *et al.*,
399 2016). The viral protein PB1-F2 negatively regulates the NLRP3 inflammasome (Yoshizumi *et al.*, 2014),
400 and this could be related to its ability to stimulate mitophagy (Wang *et al.*, 2020). The activity of BHRF1
401 on the inflammasome is currently unknown but EBV encodes an miRNA that targets the *NLRP3* mRNA
402 (Haneklaus *et al.*, 2012).

403 To conclude, we demonstrated how BHRF1, which is expressed during the early stages of EBV infection
404 and some latency programs associated with lymphomas (Fitzsimmons and Kelly, 2017), reduces innate
405 immunity by manipulating the MT network. We propose a model (***Figure 7***) in which EBV exploits
406 acetylated MTs to change mitochondrial morphodynamics, thereby draining fragmented mitochondria
407 toward the centrosome, segregating them from IFN signaling pathways in mitophagosomes to block
408 IFN production and create an optimal environment for virus replication. We previously showed that
409 BHRF1 expression induces mitochondrial fission activation and subsequently autophagy stimulation
410 (Figure 7). We report here that MT hyperacetylation is downstream of these events. Beyond EBV
411 infection and latency, these findings identify for the first time a role for acetylated MTs in regulating
412 IFN response and innate immunity against viruses.

413 ## Materials and methods

414 ### Antibodies

415 Primary antibodies used in this study included anti-β-actin (Merck Millipore, MAB1501), anti-BHRF1
416 (Merck Millipore, MAB8188), anti-c-Myc (Sigma-Aldrich, M4439), anti-HA (Santa Cruz Biotechnology,
417 sc-9082), anti-IRF3 (Novus Biologicals, SD2062), anti-LC3 (MBL International, PM036 and M151-3B),
418 anti-pericentrin (Sigma-Aldrich, HPA016820), anti-TOM20 (BD Biosciences, 612278), anti-α-tubulin
419 (Sigma-Aldrich, T6199) and anti-acetyl-α-tubulin (Sigma-Aldrich, T6793). Secondary antibodies used in
420 this study included Alexa Fluor 488 goat anti-rabbit, anti-mouse (Jackson ImmunoResearch, 111-545-
421 003, 115-545-003), Alexa Fluor 555 goat anti-rabbit, anti-mouse (Life technology, A21428, A21424),
422 Alexa Fluor 647 donkey anti-rabbit, anti-mouse (Life technology, A31573, A31571). Horseradish
423 peroxidase (HRP)-labeled goat anti-mouse and anti-rabbit secondary antibodies were purchased from
424 Jackson ImmunoResearch Laboratories (115–035–003, 111–035–003).

425 ### Cell culture and transfection

426 HeLa and HEK293T cells were cultured at 37°C under 5% CO_2 in Dulbecco's modified eagle medium
427 (DMEM; Gibco, 41965-039) supplemented with 10% fetal calf serum (FCS; Dominique Dutscher, S181B-
428 500).
429 DNA plasmid transfections were performed using Fugene HD transfection reagent (Promega
430 Corporation, E2311) according to the manufacturer's protocol. One day prior to transfection, cells
431 were seeded in 24-well plates and incubated at 37°C. On the day of transfection, DNA plasmids were
432 dispersed in opti-MEM (Gibco, 31985-047) and Fugene HD was added to the mix (ratio DNA:Fugene
433 equals 1:3). After incubation for 10 min at room temperature (RT), the transfection mix was added to
434 the cells. Then cells were incubated at 37°C and 6 h post-transfection, DMEM supplemented with 10%
435 FCS was added. Depending on the expression plasmids, cells were fixed 24 h or 48 h post-transfection.

436 ### Extinction of ATAT1 expression

437 To deplete ATAT1 in HeLa cells, we performed transfection of siRNA directed against ATAT1 encoding
438 mRNA (or non-relevant siRNA as control). We used ON-TARGETplus siRNAs from Dharmacon as a pool
439 of four siRNAs: 5-GUAGCUAGGUCCCGAUAUA-3; 5-GAGUAUAGCUAGAUCCCUU-3; 5-
440 GGGAAACUCACCAGAA CGA-3; and 5-CUUGUGAGAUUGUCGAGAU-3. The transfections of siRNA were
441 performed using Oligofectamine reagent (Thermo Fisher Scientific; 12.252.011) according to the
442 manufacturer's protocol and were repeated at days 1, 2, and 3 at a final concentration of 100 nM. At
443 the end of day 3, transfection with BHRF1-HA was also performed using Fugene HD transfection
444 reagent as described above. Cells were then used at day 4 for immunoblotting or immunofluorescence
445 analyses.

446 ***In vitro* tubulin deacetylation assay**

447 Cell lysates of control cells or cells transfected with BHRF1-HA plasmids were prepared using 10 mM
448 Tris buffer pH 8.0, supplemented with 1% Triton, 1 mM NAD^+, and the protease inhibitor cocktail.
449 Lysate aliquots containing 20 µg of proteins were mixed with 2 µg of soluble acetylated tubulin dimers
450 purified from porcine brain (Mackeh *et al.*, 2014; Walker *et al.*, 1988) and adjusted to 50 µL with NAD^+-
451 containing PEM buffer (80 mM PIPES, 2 mM EGTA, 1 mM $MgCl_2$). After 1 h at 37°C, reactions were
452 stopped by adding 4X SDS-PAGE sample buffer and immediately subjected to SDS-PAGE and Western
453 blotting of acetylated and total α-tubulin.

454 **Immunoblot analysis**

455 Cells were lysed in lysis buffer (65 mM Tris, pH 6.8, 4% SDS, 1.5% β-mercaptoethanol, and a cocktail of
456 protease/phosphatase inhibitors) and kept at 100°C for 10 min. Protein extracts were resolved on SDS-
457 PAGE (12.5%) and electro-transferred onto a polyvinylidene difluoride membrane (Amersham,
458 10600002). After 1h of incubation in blocking buffer (PBS, 0.1% Tween20, and 5% BSA or nonfat dry
459 milk), the membranes were probed overnight at 4°C with primary antibodies. Horseradish peroxidase-
460 labeled antibodies were used as secondary antibody, and revelation was performed using the ECL
461 detection system according to the manufacturer's instructions (Merck Millipore, WBKLS0500).
462 Scanning for quantification of protein levels was monitored using ImageJ software. An anti-β-actin
463 antibody was used to ensure equal loadings and normalize quantification.

464 **Immunofluorescence analysis**

465 For all indirect immunofluorescence, cells were cultured on glass coverslips in 24-well plates. Cell
466 monolayers were washed with PBS and cells were fixed with paraformaldehyde (PFA; 4%) in PBS or
467 methanol, depending on the antibodies. The cells were treated with PBS containing NH_4Cl (50 mM) for
468 10 min, permeabilized using PBS, Triton X-100 (0.2%) for 4 min, washed twice with PBS and then
469 incubated for 1 h in PBS, gelatin (0.2%) supplemented with FCS (5%) for blocking. Then the cells were
470 incubated for 1 h with the appropriate primary antibody diluted in PBS, gelatin (0.2%) at RT. Cells were
471 washed three times with PBS and then incubated with the appropriate secondary antibody diluted in
472 PBS, gelatin (0.2%) for 1 h at RT. After washing, the nuclei were counterstained with DAPI. Coverslips
473 were mounted in Glycergel (Agilent Dako, C056330-2) and observed using a Nikon Eclipse 80i
474 epifluorescence microscope (Nikon Instruments) or a Leica TCS SP8 X inverted confocal microscope
475 (Leica, USA). Photographic images were resized, organized, and labeled using Fiji-ImageJ software or
476 LAS AF Lite. Imaris software was also used to perform 3D reconstruction video.
477 A specific procedure was performed for the colocalization study between mitochondria and
478 autophagosomes. Permeabilization and blocking were performed by incubating the cells for 30 min

479 with PBS, saponin (0.075%; Sigma-Aldrich, 84,510), BSA (1%), and FCS (5%). Antibodies were diluted in
480 PBS, saponin (0.075%), and BSA (1%). In addition, between each antibody incubation, cells were
481 washed twice in PBS, saponin (0.075%), BSA (1%), once with PBS, saponin (0.037%), BSA (0.5%) and
482 twice in PBS. Other steps were the same as described above.

483 **Luciferase reporter assays to assess IFN-β promoter activity**

484 HEK293T cells were cultured in 24-well plates and transfected for 24 h using Fugene HD, with plasmids
485 encoding the IFN-β luciferase reporter (firefly luciferase; 100 ng), pRL-TK (renilla luciferase; 25 ng),
486 pΔRIG-I (2xCARD) (encoding a positive dominant form of RIG-I; 150 ng), plasmids expressing BHRF1-
487 HA (or EV as control; 150 ng) and mCherry-Tub (WT or K40A; 150 ng). One day after transfection, cells
488 were lysed and measurement of firefly and renilla luciferase activities was performed using the dual-
489 luciferase reporter assay system (Promega Corporation, E1910) according to the manufacturer's
490 protocol. Relative expression levels were calculated by dividing the firefly luciferase values by those of
491 renilla luciferase and normalized to the control condition (without BHRF1-HA expression).

492 **Microtubules depolymerization and repolymerization**

493 To depolymerize MTs, HeLa cells were seeded directly onto glass coverslips and incubated one day
494 before being transfected to express BHRF1. Twenty-four hours after transfection, cells were treated
495 with 10 µM nocodazole (Sigma-Aldrich, M1404) for 2 h at 37°C then 1.5 h at 4°C, to depolymerize the
496 MT network. Cells were immediately PFA 4% fixed and then methanol-permeabilized (t = 0 h before
497 repolymerization). MTs and mitochondria were visualized by immunostaining of α-tubulin and TOM20,
498 respectively. To allow reassembly of the MT network, nocodazole was removed by repeated washes
499 with PBS, and cells were left 1 h in warm complete medium (t = 1 h after MTs regrowth). Cells were
500 then immunostained for BHRF1, TOM20, and α-tubulin.

501 **Mitochondrial phenotype assessment**

502 BHRF1-induced mito-aggresomes were scored by measuring the CI of mitochondrial staining, as we
503 previously described (Vilmen *et al.*, 2020), based on Narendra et al. study (Narendra *et al.*, 2010). We
504 arbitrary determined that a cell presents a mito-aggresome when the CI is above 0.4. The percentage
505 of cells presenting a mito-aggresome was determined by counting at least 20 random cells in each
506 condition from three independent experiments.
507 Mitochondrial morphology was assessed by measuring AR and FF, which are indicators of
508 mitochondrial length and branching, respectively. These parameters were quantified as described
509 before (Koopman *et al.*, 2006). Briefly, on Fiji-ImageJ software, images of mitochondria were convolved
510 using the matrix developed by Koopman, then a threshold was applied to isolate mitochondria from
511 background. Then cell outline was drawn and mitochondrial phenotype was assessed by the

512 implement analysis particle tool. The AR value is given by the software and corresponds to the ratio
513 between the major and minor axis of the ellipsis equivalent to the mitochondria. The FF value is defined
514 as $(P_{mit}^2)/(4\pi A_{mit})$, where P_{mit} is the length of mitochondrial outline and A_{mit} is the area of mitochondria.
515 The mitochondrial fission parameters were determined by analyzing at least 15 random cells in each
516 condition from three independent experiments.

517 **Plasmids**

518 We previously described the BHRF1-HA expression vector (Vilmen *et al.*, 2020), which was constructed
519 from a pcDNA3.1 expression vector (EV) purchased from Invitrogen (V79020). The mCherry-α-tubulin
520 WT-K40K control vector was kindly provided by Dr. R. Y. Tsien (Department of Pharmacology, Howard
521 Hughes Medical Center, University of San Diego, USA) (Shaner *et al.*, 2004) and the mutated vector
522 (mCherry-α-tubulin K40A) was a kind gift from Dr. F. Saudou (Institut Curie, Orsay, France) (Dompierre
523 *et al.*, 2007). The plasmids Flag-ΔRIG-I (2xCARD) and pIFN-β-Luc were previously described respectively
524 (Yoneyama *et al.*, 2004, 1996) and kindly provided by Dr. C. Lagaudrière (I2BC, Gif-sur-Yvette, France).
525 The plasmid pRL-TK was purchased from Promega Corporation (E2241). The p50-dynamitin construct
526 was a gift from Dr. S. Etienne-Manneville (Institut Pasteur, Paris, France) (Etienne-Manneville and Hall,
527 2001).

528 **Reagents**

529 MitoTracker Red CMXRos was purchased from Life Technologies (M7512) and used at 100 nM for 30
530 min before cell fixation to stain the mitochondrial network. Phalloidin–Tetramethylrhodamine B
531 isothiocyanate was purchased from Sigma-Aldrich (P1951) and used at 20 µg/mL during 1 h to stain F-
532 actin. DAPI was purchased from Thermo Fisher Scientific (D1306) and used at 300 nM to stain dsDNA
533 (nuclei). Nocodazole was purchased from Sigma-Aldrich (M1404) and used at 10 µM to disrupt the MT
534 network. Ciliobrevin D was purchased from Sigma-Aldrich (250401) and used at 40 µM overnight to
535 inhibit cytosolic dyneins. Cytochalasin B was purchased from Sigma-Aldrich (C6762) and used at 10
536 µg/mL for 30 min to disrupt F-actin. Autophagic flux was monitored by the addition of chloroquine
537 (Sigma-Aldrich, C6628) at 50 µM for 2 to 4 h. To inhibit autophagy, we used two different ways: cells
538 were treated either with 3-MA (Sigma-Aldrich, M9281) at 5 mM for 8 h or by spautin-1 (Sigma-Aldrich,
539 SML0440) at 20 µM for 8 h.

540 **Results quantification**

541 The number of endogenous LC3 dots per cell was determined using Fiji-ImageJ software. All images
542 were taken with the same microscope settings to allow for comparison. Images were converted into
543 8-bit. Cells' outlines were drawn and nuclei cropped to conserve only the cytoplasm. A thresholding of
544 images was performed to detect only LC3 vesicles. Note that the value of the threshold was conserved

545 and used for each analyzed cell. Finally, the "analyze particles" plug-in was used to count the total
546 number of LC3 dots per cell. For each condition, at least 25 cells were analyzed in three independent
547 experiments.
548 The colocalization degree between mitochondrial staining and autophagosomes staining was assessed
549 by measuring Manders split coefficient using the "colocalization threshold" plug-in on Fiji-ImageJ
550 software. For each condition, 30 random cells were analyzed.
551 The proportion of cells presenting an IRF3 nuclear localization was determined by counting at least 50
552 random cells in each condition from three independent experiments.

553 **Statistical analysis**

554 Data are expressed as mean ± standard error of the mean (SEM) and were analyzed with Prism
555 software (GraphPad) by using Student's t-test. P values less than 0.05 were considered statistically
556 significant. Data from three independent experiments were analysed.

557 Acknowledgments

558 We would like to thank for her technical assistance Valérie Nicolas (Université Paris-Saclay, Châtenay-
559 Malabry, France) from the MIPSIT cellular imaging facility. Also, the present work has benefited from
560 the core facilities of Imagerie-Gif, (http://www.i2bc.paris-saclay.fr), member of IBiSA
561 (http://www.ibisa.net), supported by "France-BioImaging" (ANR- 10-INBS-04-01), and the Labex
562 "Saclay Plant Science" (ANR-11- IDEX-0003-02). Finally, we thank Stephanie Straubel for critical reading
563 of the manuscript.

564 Additional information

565 Funding

Funder	Grand reference number	Author
CNRS, Univ Paris-Sud, DIM MALINF Région IDF	N/A	Géraldine Vilmen
Agence Nationale de la Recherche	ANR-14-CE14-0022	Audrey Esclatine

The authors declare that the funders had no role in study design, data collection or interpretation, or the decision to submit the work for publication.

566

567 Author contributions

568 DG, GV, DP, conception and design, investigation, formal analysis, writing original draft; EH,
569 investigation, formal analysis; GB, formal analysis, writing original draft, VM, formal analysis, funding
570 acquisition, supervision; CP, formal analysis, provided materials; ML, conception and design, formal

571 analysis, writing original draft, supervision; AE, conception and design, formal analysis, funding
572 acquisition, writing original draft, supervision.

573 ## Authors ORCIDs

574 Damien Glon : https://orcid.org/0000-0001-8405-8805
575 Guillaume Beauclair : https://orcid.org/0000-0001-5323-5987
576 Vincent Maréchal : https://orcid.org/0000-0003-2689-6266
577 Christian Poüs : https://orcid.org/0000-0002-2502-7854
578 Marion Lussignol : https://orcid.org/0000-0001-7586-2041

579 ## Supplementary files

580 - Supplementary file 1. BHRF1 localizes in proximity of the centrosome.
581 - Supplementary file 2. The actin network is not involved in the formation of BHRF1-induced mito-
582 aggresomes.
583 - Supplementary file 3. Expression of the non-acetylatable α-tubulin K40A does not impact
584 mitochondrial network.
585 - Supplementary file 4. Dyneins inhibition prevents BHRF1-induced mito-aggresomes.
586 - Supplementary file 5. BHRF1 stimulates autophagy when α-tubulin WT is expressed, and
587 autophagy is required to MT hyperacetylation.
588 - Supplementary file 6. Full-length western-blots.

589 ## Data availability

590 All data generated or analyzed during this study are included in this published article and its
591 supplementary information files.

592 ## References

Arnoult D, Soares F, Tattoli I, Girardin SE. 2011. Mitochondria in innate immunity. *EMBO Rep* **12**:901–910. doi:10.1038/embor.2011.157

Castanier C, Garcin D, Vazquez A, Arnoult D. 2010. Mitochondrial dynamics regulate the RIG-I-like receptor antiviral pathway. *EMBO Rep* **11**:133–138. doi:10.1038/embor.2009.258

Chatel-Chaix L, Cortese M, Romero-Brey I, Bender S, Neufeldt CJ, Fischl W, Scaturro P, Schieber N, Schwab Y, Fischer B, Ruggieri A, Bartenschlager R. 2016. Dengue Virus Perturbs Mitochondrial Morphodynamics to Dampen Innate Immune Responses. *Cell Host Microbe* **20**:342–356. doi:10.1016/j.chom.2016.07.008

De Vos KJ, Allan VJ, Grierson AJ, Sheetz MP. 2005. Mitochondrial Function and Actin Regulate Dynamin-Related Protein 1-Dependent Mitochondrial Fission. *Curr Biol* **15**:678–683. doi:10.1016/j.cub.2005.02.064

Desbien AL, Kappler JW, Marrack P. 2009. The Epstein-Barr virus Bcl-2 homolog, BHRF1, blocks apoptosis by binding to a limited amount of Bim. *Proc Natl Acad Sci U S A* **106**:5663–5668. doi:10.1073/pnas.0901036106

Detmer SA, Chan DC. 2007. Functions and dysfunctions of mitochondrial dynamics. *Nat Rev Mol Cell Biol* **8**:870–879. doi:10.1038/nrm2275
Ding B, Zhang L, Li Z, Zhong Y, Tang Q, Qin Y, Chen M. 2017. The Matrix Protein of Human Parainfluenza Virus Type 3 Induces Mitophagy that Suppresses Interferon Responses. *Cell Host & Microbe* **21**:538-547.e4. doi:10.1016/j.chom.2017.03.004
Dompierre JP, Godin JD, Charrin BC, Cordelieres FP, King SJ, Humbert S, Saudou F. 2007. Histone Deacetylase 6 Inhibition Compensates for the Transport Deficit in Huntington's Disease by Increasing Tubulin Acetylation. *J Neurosci* **27**:3571–3583. doi:10.1523/JNEUROSCI.0037-07.2007
Eshun-Wilson L, Zhang R, Portran D, Nachury MV, Toso DB, Löhr T, Vendruscolo M, Bonomi M, Fraser JS, Nogales E. 2019. Effects of α-tubulin acetylation on microtubule structure and stability. *Proc Natl Acad Sci U S A* **116**:10366–10371. doi:10.1073/pnas.1900441116
Esteves AR, Palma AM, Gomes R, Santos D, Silva DF, Cardoso SM. 2019. Acetylation as a major determinant to microtubule-dependent autophagy: Relevance to Alzheimer's and Parkinson disease pathology. *Biochim Biophys Acta*, Post-Translational Modifications In Brain Health And Disease **1865**:2008–2023. doi:10.1016/j.bbadis.2018.11.014
Etienne-Manneville S, Hall A. 2001. Integrin-mediated activation of Cdc42 controls cell polarity in migrating astrocytes through PKCzeta. *Cell* **106**:489–498. doi:10.1016/s0092-8674(01)00471-8
Fitzsimmons L, Kelly G. 2017. EBV and Apoptosis: The Viral Master Regulator of Cell Fate? *Viruses* **9**:339–373. doi:10.3390/v9110339
Fransson Å, Ruusala A, Aspenström P. 2006. The atypical Rho GTPases Miro-1 and Miro-2 have essential roles in mitochondrial trafficking. *Biochem Biophys Res Commun* **344**:500–510. doi:10.1016/j.bbrc.2006.03.163
Frederick RL, Shaw JM. 2007. Moving Mitochondria: Establishing Distribution of an Essential Organelle. *Traffic* **8**:1668–1675. doi:10.1111/j.1600-0854.2007.00644.x
Friedman JR, Lackner LL, West M, DiBenedetto JR, Nunnari J, Voeltz GK. 2011. ER Tubules Mark Sites of Mitochondrial Division. *Science* **334**:358–362. doi:10.1126/science.1207385
Friedman JR, Webster BM, Mastronarde DN, Verhey KJ, Voeltz GK. 2010. ER sliding dynamics and ER–mitochondrial contacts occur on acetylated microtubules. *J Cell Biol* **190**:363–375. doi:10.1083/jcb.200911024
Geeraert C, Ratier A, Pfisterer SG, Perdiz D, Cantaloube I, Rouault A, Pattingre S, Proikas-Cezanne T, Codogno P, Poüs C. 2010. Starvation-induced Hyperacetylation of Tubulin Is Required for the Stimulation of Autophagy by Nutrient Deprivation. *J Biol Chem* **285**:24184–24194. doi:10.1074/jbc.M109.091553
Giacomello M, Pyakurel A, Glytsou C, Scorrano L. 2020. The cell biology of mitochondrial membrane dynamics. *Nat Rev Mol Cell Biol* **21**:204–224. doi:10.1038/s41580-020-0210-7
Green DR, Levine B. 2014. To Be or Not to Be? How Selective Autophagy and Cell Death Govern Cell Fate. *Cell* **157**:65–75. doi:10.1016/j.cell.2014.02.049
Hancock WO. 2014. Bidirectional cargo transport: moving beyond tug of war. *Nat Rev Mol Cell Biol* **15**:615–628. doi:10.1038/nrm3853
Haneklaus M, Gerlic M, Kurowska-Stolarska M, Rainey A-A, Pich D, McInnes IB, Hammerschmidt W, O'Neill LAJ, Masters SL. 2012. Cutting Edge: miR-223 and EBV miR-BART15 Regulate the NLRP3 Inflammasome and IL-1β Production. *J Immunol* **189**:3795–3799. doi:10.4049/jimmunol.1200312
Hubbert C, Guardiola A, Shao R, Kawaguchi Y, Ito A, Nixon A, Yoshida M, Wang X-F, Yao T-P. 2002. HDAC6 is a microtubule-associated deacetylase. *Nature* **417**:455–458. doi:10.1038/417455a
Janke C, Magiera MM. 2020. The tubulin code and its role in controlling microtubule properties and functions. *Nat Rev Mol Cell Biol* **21**:307–326. doi:10.1038/s41580-020-0214-3
Janke C, Montagnac G. 2017. Causes and Consequences of Microtubule Acetylation. *Curr Biol* **27**:1287–1292. doi:10.1016/j.cub.2017.10.044

Kaufmann T, Kukolj E, Brachner A, Beltzung E, Bruno M, Kostrhon S, Opravil S, Hudecz O, Mechtler K, Warren G, Slade D. 2016. SIRT2 regulates nuclear envelope reassembly through ANKLE2 deacetylation. *J Cell Sci* **129**:4607–4621. doi:10.1242/jcs.192633

Khanim F, Mackett M, Young LS, Dawson J, Meseda CA, Dawson C. 1997. BHRF1, a viral homologue of the Bcl-2 oncogene, is conserved at both the sequence and functional level in different Epstein-Barr virus isolates. *J Gen Virol* **78**:2987–2999. doi:10.1099/0022-1317-78-11-2987

Köchl R, Hu XW, Chan EYW, Tooze SA. 2006. Microtubules Facilitate Autophagosome Formation and Fusion of Autophagosomes with Endosomes: Role of Microtubules in AV Formation. *Traffic* **7**:129–145. doi:10.1111/j.1600-0854.2005.00368.x

Koopman WJH, Visch H-J, Smeitink JAM, Willems PHGM. 2006. Simultaneous quantitative measurement and automated analysis of mitochondrial morphology, mass, potential, and motility in living human skin fibroblasts. *Cytometry Part A* **69A**:1–12. doi:10.1002/cyto.a.20198

Kruppa AJ, Buss F. 2021. Motor proteins at the mitochondria-cytoskeleton interface. *J Cell Sci* **134**:1–13. doi:10.1242/jcs.226084

Kvansakul M, Wei AH, Fletcher JI, Willis SN, Chen L, Roberts AW, Huang DCS, Colman PM. 2010. Structural Basis for Apoptosis Inhibition by Epstein-Barr Virus BHRF1. *PLoS Pathog* **6**:e1001236. doi:10.1371/journal.ppat.1001236

Lee AJ, Ashkar AA. 2018. The Dual Nature of Type I and Type II Interferons. *Front Immunol* **9**:2061–2070. doi:10.3389/fimmu.2018.02061

Lee J-Y, Nagano Y, Taylor JP, Lim KL, Yao T-P. 2010. Disease-causing mutations in Parkin impair mitochondrial ubiquitination, aggregation, and HDAC6-dependent mitophagy. *J Cell Biol* **189**:671–679. doi:10.1083/jcb.201001039

Li L, Yang X-J. 2015. Tubulin acetylation: responsible enzymes, biological functions and human diseases. *Cell Mol Life Sci* **72**:4237–4255. doi:10.1007/s00018-015-2000-5

López-Doménech G, Covill-Cooke C, Ivankovic D, Halff EF, Sheehan DF, Norkett R, Birsa N, Kittler JT. 2018. Miro proteins coordinate microtubule- and actin-dependent mitochondrial transport and distribution. *EMBO J* **37**:321–336. doi:10.15252/embj.201696380

Luo S, Garcia-Arencibia M, Zhao R, Puri C, Toh PPC, Sadiq O, Rubinsztein DC. 2012. Bim inhibits autophagy by recruiting Beclin 1 to microtubules. *Mol Cell* **47**:359–370. doi:10.1016/j.molcel.2012.05.040

Mackeh R, Lorin S, Ratier A, Mejdoubi-Charef N, Baillet A, Bruneel A, Hamaï A, Codogno P, Poüs C, Perdiz D. 2014. Reactive Oxygen Species, AMP-activated Protein Kinase, and the Transcription Cofactor p300 Regulate α-Tubulin Acetyltransferase-1 (αTAT-1/MEC-17)-dependent Microtubule Hyperacetylation during Cell Stress. *J Biol Chem* **289**:11816–11828. doi:10.1074/jbc.M113.507400

Mackeh R, Perdiz D, Lorin S, Codogno P, Pous C. 2013. Autophagy and microtubules - new story, old players. *J Cell Sci* **126**:1071–80. doi:10.1242/jcs.115626

Misawa T, Takahama M, Kozaki T, Lee H, Zou J, Saitoh T, Akira S. 2013. Microtubule-driven spatial arrangement of mitochondria promotes activation of the NLRP3 inflammasome. *Nat Immunol* **14**:454–460. doi:10.1038/ni.2550

Mishra SR, Mahapatra KK, Behera BP, Patra S, Bhol CS, Panigrahi DP, Praharaj PP, Singh A, Patil S, Dhiman R, Bhutia SK. 2021. Mitochondrial dysfunction as a driver of NLRP3 inflammasome activation and its modulation through mitophagy for potential therapeutics. *Int J Biochem Cell Biol* **136**:106013–106021. doi:10.1016/j.biocel.2021.106013

Narendra D, Kane LA, Hauser DN, Fearnley IM, Youle RJ. 2010. p62/SQSTM1 is required for Parkin-induced mitochondrial clustering but not mitophagy; VDAC1 is dispensable for both. *Autophagy* **6**:1090–1106. doi:10.4161/auto.6.8.13426

North BJ, Marshall BL, Borra MT, Denu JM, Verdin E. 2003. The Human Sir2 Ortholog, SIRT2, Is an NAD+-Dependent Tubulin Deacetylase. *Mol Cell* **11**:437–444. doi:10.1016/s1097-2765(03)00038-8

Nowosad A, Creff J, Jeannot P, Culerrier R, Codogno P, Manenti S, Nguyen L, Besson A. 2021. p27 controls autophagic vesicle trafficking in glucose-deprived cells via the regulation of ATAT1-mediated microtubule acetylation. *Cell Death Dis* **12**:1–18. doi:10.1038/s41419-021-03759-9

Pagliuso A, Cossart P, Stavru F. 2018. The ever-growing complexity of the mitochondrial fission machinery. *Cell Mol Life Sci* **75**:355–374. doi:10.1007/s00018-017-2603-0

Perdiz D, Lorin S, Leroy-Gori I, Poüs C. 2017. Stress-induced hyperacetylation of microtubule enhances mitochondrial fission and modulates the phosphorylation of Drp1 at 616 Ser. *Cell Signalling* **39**:32–43. doi:10.1016/j.cellsig.2017.07.020

Perdiz D, Mackeh R, Poüs C, Baillet A. 2011. The ins and outs of tubulin acetylation: More than just a post-translational modification? *Cell Signalling* **23**:763–771. doi:10.1016/j.cellsig.2010.10.014

Portran D, Schaedel L, Xu Z, Théry M, Nachury MV. 2017. Tubulin acetylation protects long-lived microtubules against mechanical ageing. *Nat Cell Biol* **19**:391–398. doi:10.1038/ncb3481

Puthalakath H, Huang DCS, O'Reilly LA, King SM, Strasser A. 1999. The Proapoptotic Activity of the Bcl-2 Family Member Bim Is Regulated by Interaction with the Dynein Motor Complex. *Mol Cell* **3**:287–296. doi:10.1016/S1097-2765(00)80456-6

Reed NA, Cai D, Blasius TL, Jih GT, Meyhofer E, Gaertig J, Verhey KJ. 2006. Microtubule Acetylation Promotes Kinesin-1 Binding and Transport. *Curr Biol* **16**:2166–2172. doi:10.1016/j.cub.2006.09.014

Roberts AJ, Kon T, Knight PJ, Sutoh K, Burgess SA. 2013. Functions and mechanics of dynein motor proteins. *Nat Rev Mol Cell Biol* **14**:713–726. doi:10.1038/nrm3667

Shaner NC, Campbell RE, Steinbach PA, Giepmans BNG, Palmer AE, Tsien RY. 2004. Improved monomeric red, orange and yellow fluorescent proteins derived from Discosoma sp. red fluorescent protein. *Nat Biotechnol* **22**:1567–1572. doi:10.1038/nbt1037

Shida T, Cueva JG, Xu Z, Goodman MB, Nachury MV. 2010. The major α-tubulin K40 acetyltransferase αTAT1 promotes rapid ciliogenesis and efficient mechanosensation. *Proc Natl Acad Sci U S A* **107**:21517–21522. doi:10.1073/pnas.1013728107

Singh PK, Weber A, Häcker G. 2018. The established and the predicted roles of dynein light chain in the regulation of mitochondrial apoptosis. *Cell Cycle* **17**:1037–1047. doi:10.1080/15384101.2018.1464851

Tang B. 2018. Miro—Working beyond Mitochondria and Microtubules. *Cells* **7**:18–24. doi:10.3390/cells7030018

Vilmen G, Glon D, Siracusano G, Lussignol M, Shao Z, Hernandez E, Perdiz D, Quignon F, Mouna L, Poüs C, Gruffat H, Maréchal V, Esclatine A. 2020. BHRF1, a BCL2 viral homolog, disturbs mitochondrial dynamics and stimulates mitophagy to dampen type I IFN induction. *Autophagy* ***17***:1296–1315. doi:10.1080/15548627.2020.1758416

Walker RA, O'Brien E. T, Pryer NK, Soboeiro MF, Voter WA, Erickson HP, Salmon ED. 1988. Dynamic instability of individual microtubules analyzed by video light microscopy: rate constants and transition frequencies. *J Cell Biol* **107**:1437–1448. doi:10.1083/jcb.107.4.1437

Wang K, Ma H, Liu H, Ye W, Li Z, Cheng L, Zhang L, Lei Y, Shen L, Zhang F. 2019. The Glycoprotein and Nucleocapsid Protein of Hantaviruses Manipulate Autophagy Flux to Restrain Host Innate Immune Responses. *Cell Reports* **27**:2075-2091.e5. doi:10.1016/j.celrep.2019.04.061

Wang R, Zhu Y, Ren C, Yang S, Tian S, Chen H, Jin M, Zhou H. 2020. Influenza A virus protein PB1-F2 impairs innate immunity by inducing mitophagy. *Autophagy* 1–16. doi:10.1080/15548627.2020.1725375

West AP, Shadel GS, Ghosh S. 2011. Mitochondria in innate immune responses. *Nat Rev Immunol* **11**:389–402. doi:10.1038/nri2975

Xie R, Nguyen S, McKeehan WL, Liu L. 2010. Acetylated microtubules are required for fusion of autophagosomes with lysosomes. *BMC Cell Biol* **11**:89–100. doi:10.1186/1471-2121-11-89

Yoneyama M, Kikuchi M, Natsukawa T, Shinobu N, Imaizumi T, Miyagishi M, Taira K, Akira S, Fujita T. 2004. The RNA helicase RIG-I has an essential function in double-stranded RNA-induced innate antiviral responses. *Nat Immunol* **5**:730–737. doi:10.1038/ni1087

Yoneyama M, Suhara W, Fukuhara Y, Sato M, Ozato K, Fujita T. 1996. Autocrine Amplification of Type I Interferon Gene Expression Mediated by Interferon Stimulated Gene Factor 3 (ISGF3). *J Biochem* **120**:160–169. doi:10.1093/oxfordjournals.jbchem.a021379

Yoshizumi T, Ichinohe T, Sasaki O, Otera H, Kawabata S, Mihara K, Koshiba T. 2014. Influenza A virus protein PB1-F2 translocates into mitochondria via Tom40 channels and impairs innate immunity. *Nat Commun* **5**:4713. doi:10.1038/ncomms5713

Zhao C, Zhao W. 2020. NLRP3 Inflammasome—A Key Player in Antiviral Responses. *Front Immunol* **11**. doi:10.3389/fimmu.2020.00211

Zheng K, Jiang Y, He Z, Kitazato K, Wang Y. 2017. Cellular defence or viral assist: the dilemma of HDAC6. *J Gen Virol* **98**:322–337. doi:10.1099/jgv.0.000679

Zhong Z, Umemura A, Sanchez-Lopez E, Liang S, Shalapour S, Wong J, He F, Boassa D, Perkins G, Ali SR, McGeough MG, Ellisman MH, Seki E, Gustafsson AB, Hoffman HM, Diaz-Meco MT, Moscat J, Karin M. 2016. NF-κB Restricts inflammasome activation via elimination of damaged mitochondria. *Cell* **164**:896–910. doi:10.1016/j.cell.2015.12.057

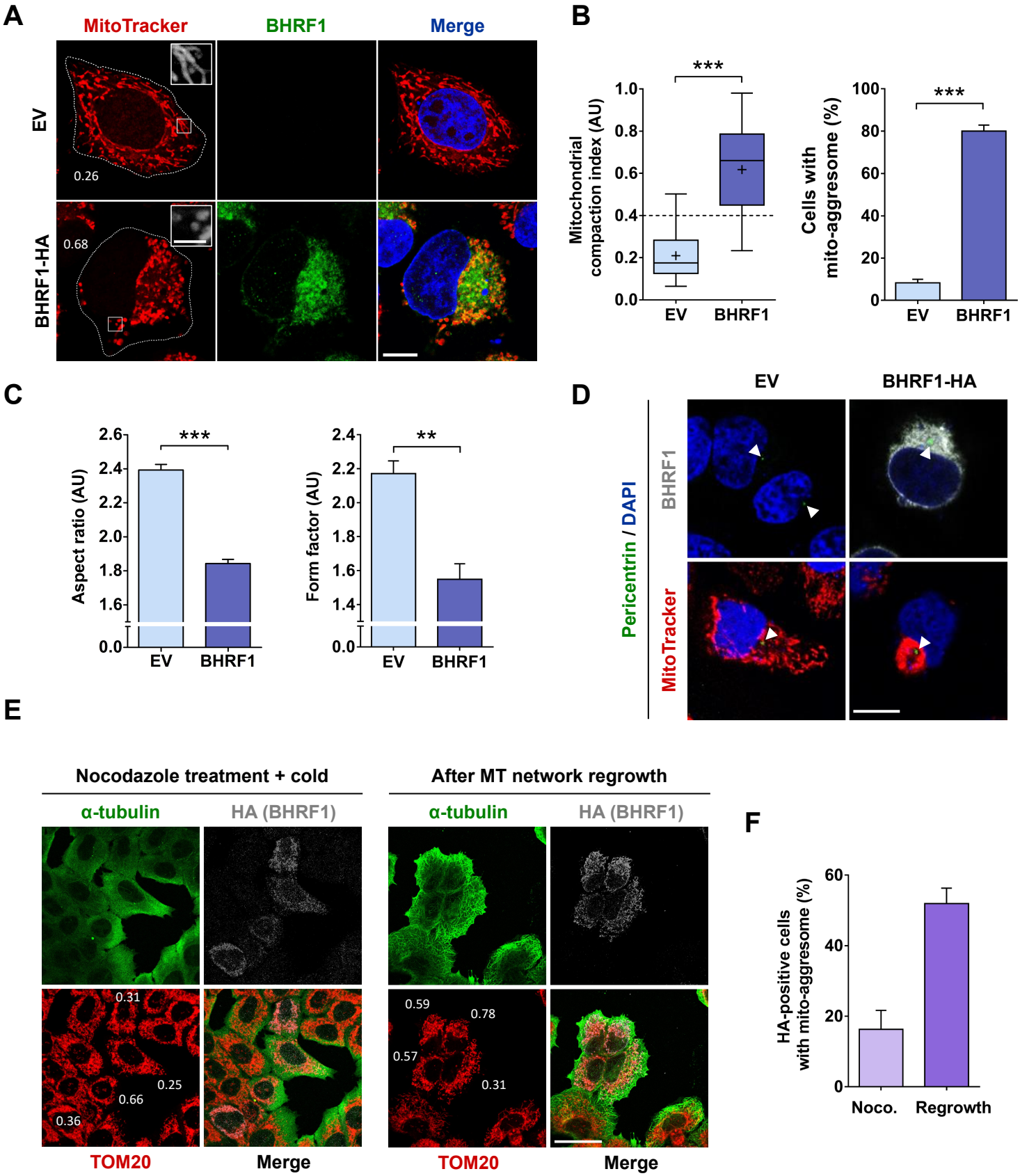

Figure 1. BHRF1 induces the formation of mito-aggresomes in a microtubule dependent manner. (**A-C**) HeLa cells were transfected for 24 h with BHRF1-HA plasmid or with EV as a control. Mitochondria were labeled with MitoTracker Red CMXRos and cells immunostained for BHRF1. Nuclei were stained with DAPI. (**A**) Confocal images with insets (3X) on mitochondrial phenotype. The values of the mitochondrial CI are indicated on representative cells. Scale bars: 10 µm, and 2 µm for insets. (**B**) *Left*, assessment of mitochondrial aggregation by calculation of CI. *Right*, percentage of cells presenting a mito-aggresome (n = 20 cells). (**C**) Quantification of mitochondrial fission parameters, aspect ratio (AR; left *panel*) and form factor (FF, *right panel*). (**D**) Confocal images of HeLa cells transfected with BHRF1-HA plasmid (or EV) and immunostained for pericentrin and BHRF1 (*upper panel*) or mitochondria (*lower panel*). Nuclei were stained with DAPI. Scale bar: 20 µm. Arrowheads show the centrosomal localization of pericentrin. (**E-F**) MT network depolymerization assay. (**E**) Representative images where BHRF1 expression is visualized by HA immunostaining (gray), the MT network by α-tubulin immunostaining (green), and mitochondria are immunostained with an anti-TOM20 antibody (red). The values of the mitochondrial CI are indicated on representative cells. Scale bars: 10 µm, and 2 µm for insets. (**F**) Percentage of BHRF1-HA-positive cells presenting a mito-aggresome (n = 30 cells) in cells treated with nocodazole and after MT regrowth. Data represent the mean ± SEM of three independent experiments. ** $P < 0.01$; *** $P < 0.001$ (Student's t-test).

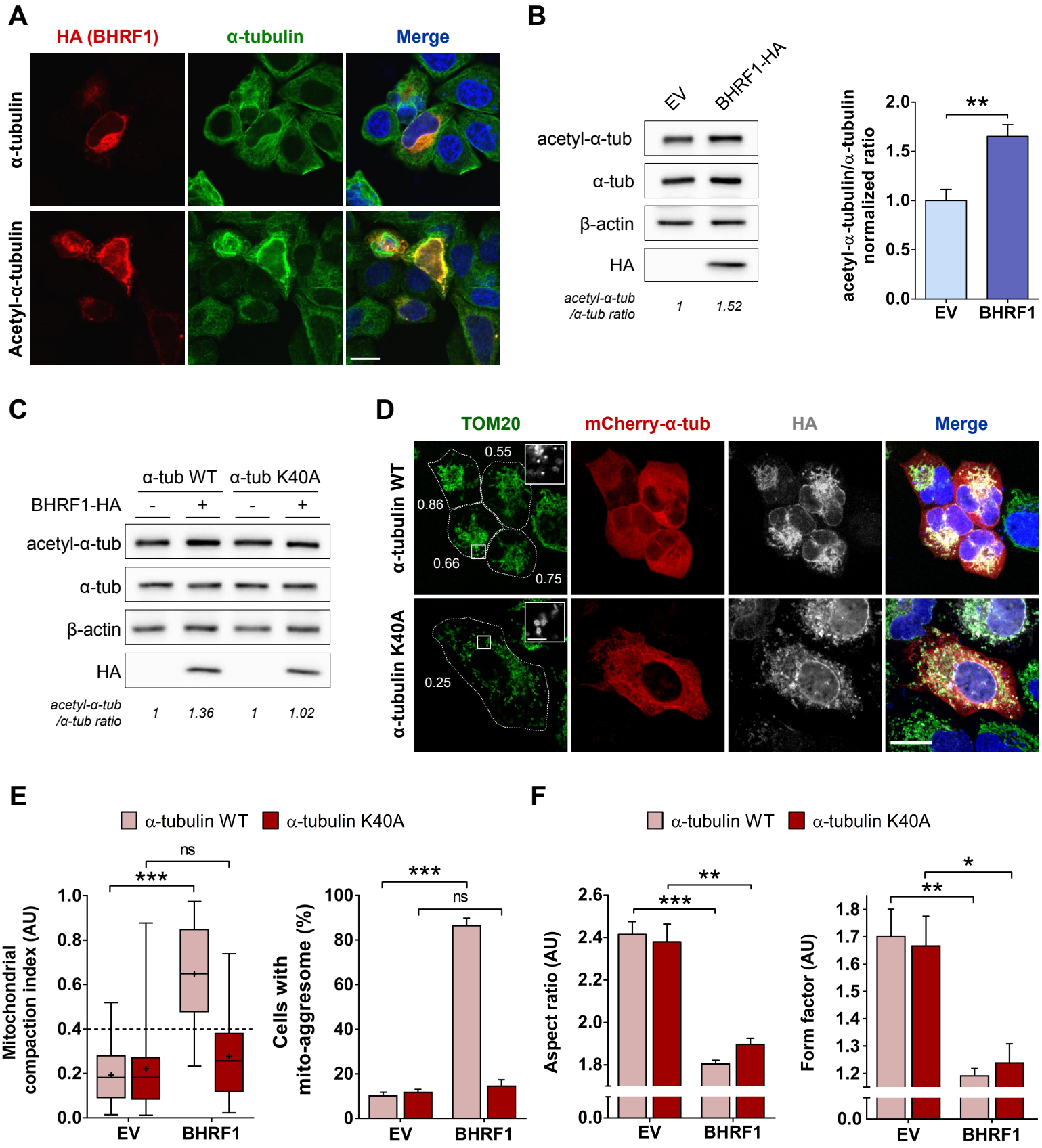

Figure 2. BHRF1 stimulates microtubules hyperacetylation, a process essential for the mito-aggresome formation. (**A**) Representative images of HeLa cells expressing BHRF1-HA and immunostained for HA and α-tubulin (*upper panel)* or acetyl-α-tubulin (*lower panel*). Nuclei were stained with DAPI. Scale bar: 20 µm. (**B**) *Left*, immunoblot analysis of BHRF1-HA, acetyl and total α-tubulin. β-actin was used as a loading control. *Right*, the histograms show the normalized ratios of acetyl-α-tubulin to total α-tubulin. (**C-F**) HeLa cells were co-transfected with plasmids encoding BHRF1-HA (or EV) and either mCherry-α-tubulin WT (K40K) or a non-acetylatable form (K40A). (**C**) Immunoblot analysis of BHRF1-HA, acetyl and total α-tubulin. (**D**) Confocal images with insets (3X). BHRF1-HA expressing cells were visualized with an anti-HA antibody and mitochondria were immunostained with an anti-TOM20 antibody. Nuclei were stained with DAPI. Scale bars: 10 µm and 4 µm for insets. Values of mitochondrial CI are indicated on representative cells. Images of control cells are presented in **Supplementary Figure 3**. (**E**) Quantification of CI and cells with mito-aggresomes (n = 20 cells). (**F**) Quantification of mitochondrial fission parameters (n = 20 cells). Data represent the mean ± SEM of three independent experiments. ns = non-significant; * $P < 0.05$; ** $P < 0.01$; *** $P < 0.001$ (Student's t-test).

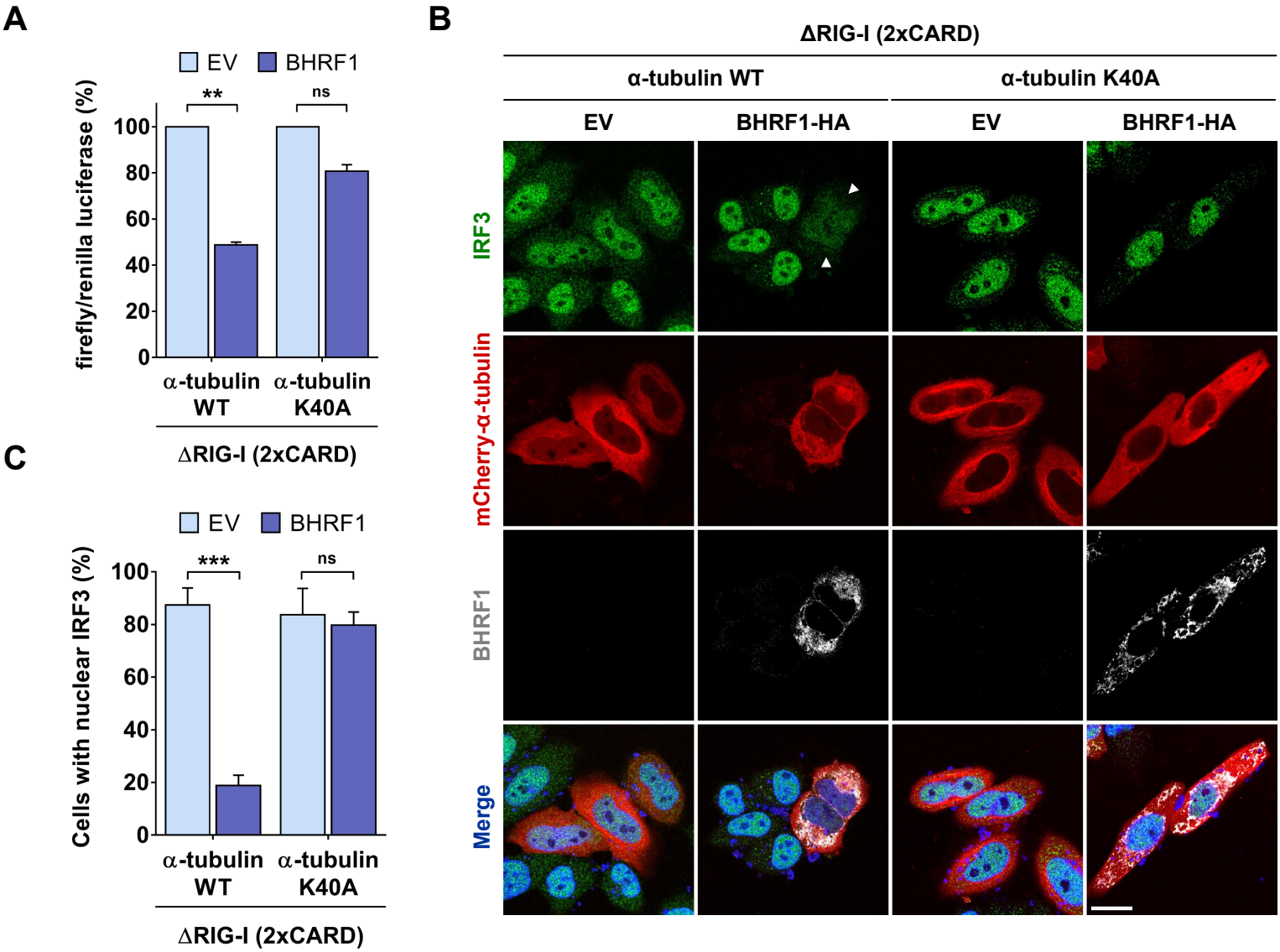

Figure 3. Hyperacetylation of α-tubulin is required for BHRF1 to block IFN. (**A**) Luciferase reporter assay on HEK293T cells co-expressing BHRF1 (or EV) and α-tubulin K40A (or WT). Activation of the IFN-β promoter was analyzed 24 h post-transfection. Firefly/renilla luciferase ratios were calculated and normalized to control conditions. (**B and C**) HeLa cells were co-transfected for 24 h with plasmids encoding BHRF1-HA (or EV), mCherry-α-tubulin K40A (or WT), and ΔRIG-I (2xCARD). (**B**) Confocal images. BHRF1-HA-transfected cells were visualized with an anti-HA antibody and cells were immunostained with an-anti IRF3 antibody. Nuclei were stained with DAPI. Scale bar: 20 µm. Arrowheads indicate BHRF1-expressing cells without IRF3 nuclear localization. (**C**) Percentage of cells expressing mCherry-α-tubulin and presenting IRF3 nuclear localization (n = 50 cells). Data represent the mean ± SEM of three independent experiments. ns = non-significant; ** $P < 0.01$; *** $P < 0.001$ (Student's t-test).

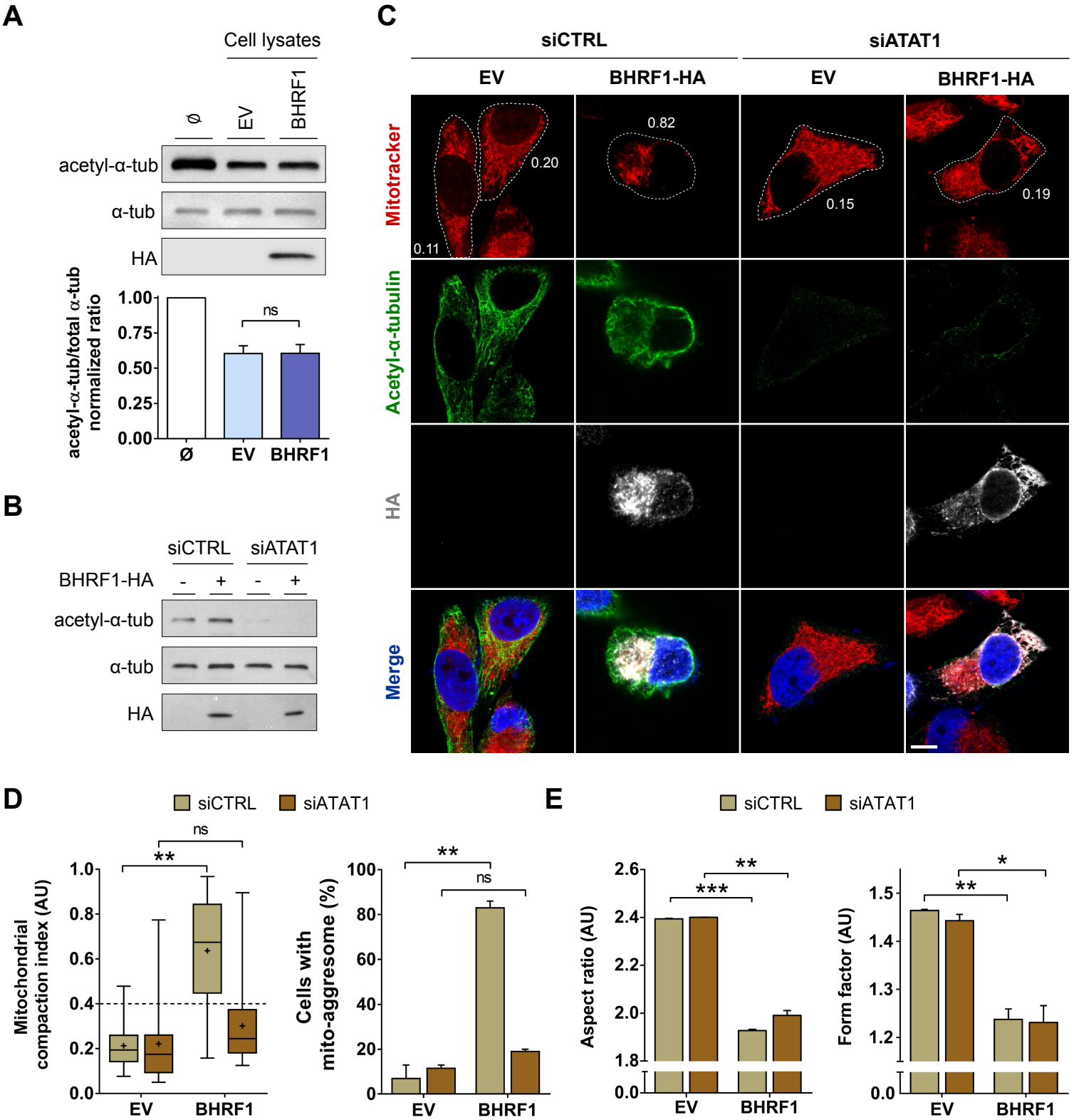

Figure 4. Characterization of MT hyperacetylation mechanism induced by BHRF1. (**A**) Tubulin deacetylation assay. HeLa cells were transfected with BHRF1-HA plasmid (or EV) and lysed 48 h post-transfection. Cell lysates were incubated *in vitro* with porcine brain tubulin and NAD+. BHRF1-HA, acetylated and total α-tubulin were detected by immunoblot, and the histogram represents the normalized ratios of acetyl to total α-tubulin. (**B-D**) After knockdown of ATAT1, HeLa cells were transfected with BHRF1-HA (or EV) and lysed/fixed 24 h post-transfection. (**B**) Extinction of ATAT1 activity visualized by immunoblot analysis of acetylated and total α-tubulin. (**C**) Confocal images. Mitochondria were labeled with MitoTracker CMXRos, and cells were immunostained for acetyl-α-tubulin and HA. Nuclei were stained with DAPI. Values of mitochondrial CI are indicated on representative cells. Scale bar: 20 µm. (**D**) Quantification of CI and cells with mito-aggresomes (n = 20 cells). (**E**) Quantification of mitochondrial fission parameters (n = 20 cells). Data represent the mean ± SEM of three independent experiments. ns = non-significant; * $P < 0.05$; ** $P < 0.01$; *** $P < 0.001$ (Student's t-test).

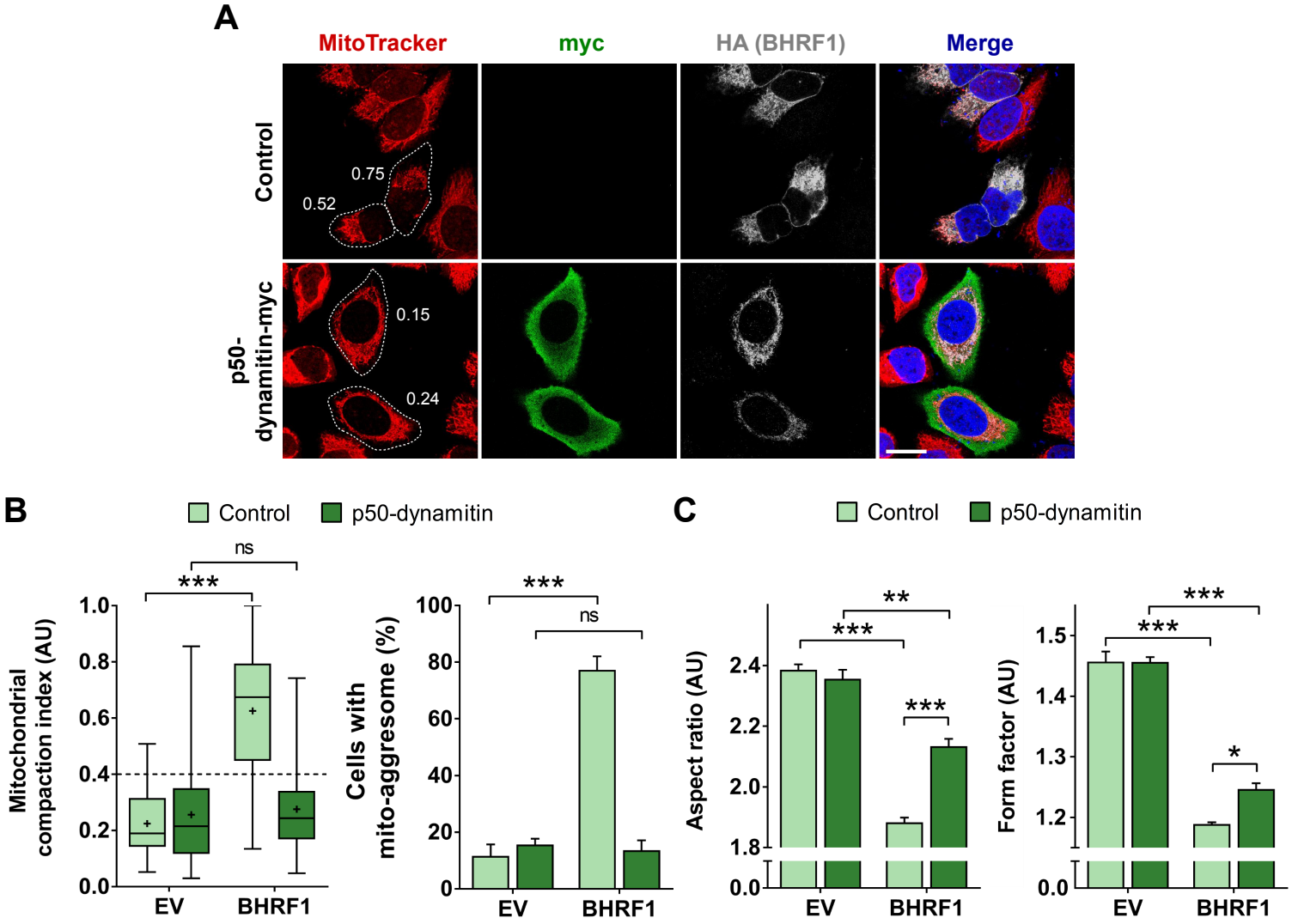

Figure 5. Dynein-based transport is required for BHRF1 to aggregate mitochondria next to the nucleus. (**A-C**) HeLa cells were co-transfected with plasmids encoding BHRF1-HA (or EV) and p50-dynamitin-myc (or control) for 24 h and then fixed. (**A**) Confocal images. Mitochondria were labeled with MitoTracker CMXRos, and cells were immunostained for c-myc and HA. Nuclei were stained with DAPI. Values of mitochondrial CI are indicated on representative cells. Scale bar: 20 µm. Images of cells expressing EV and p50-dynamitin-myc are presented in **Supplementary Figure 4A**. (**B**) Quantification of CI and cells with mito-aggresomes (n = 20 cells). (**C**) Quantification of mitochondrial fission parameters (n = 20 cells). Data represent the mean ± SEM of three independent experiments. ns = non-significant; * P < 0.05, ** P < 0.01; *** P < 0.001 (one-way ANOVA test).

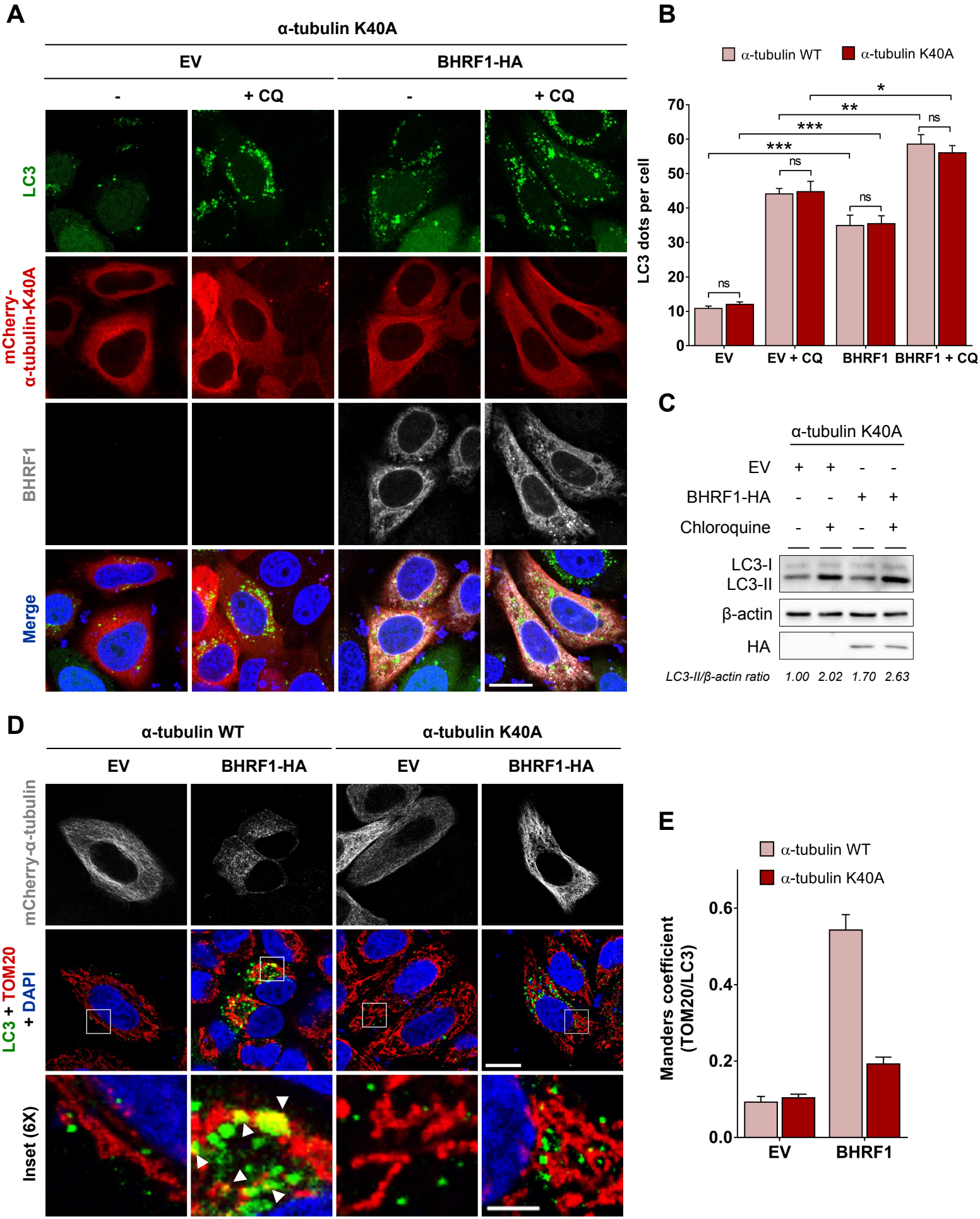

Figure 6. MT hyperacetylation is dispensable for BHRF1-pro-autophagic activity, but essential for mitophagy. (**A-C**) HeLa cells were co-transfected for 24 h with plasmids encoding BHRF1-HA (or EV) and mCherry-α-tubulin K40A (or WT), and were treated with CQ when indicated. (**A**) Confocal images. Cells were immunostained for BHRF1 and LC3 and nuclei were stained with DAPI. Scale bar: 10 µm. Images of cells transfected with mCherry-α-tubulin WT are presented in **Supplementary Figure 5A**. (**B**) Quantification of LC3 dots in each condition (n = 30 cells). (**C**) Immunoblot analysis of LC3 expression. (**D and E**) HeLa cells were co-transfected with BHRF1 (or EV) and mCherry-α-tubulin K40A (or WT). Cells were immunostained for TOM20 and LC3, and nuclei stained with DAPI. (**D**) Confocal images with insets (6X) showing colocalization events (see arrows). Scale bars: 10 µm and 5 µm for insets. (**E**) Colocalization level (Manders split coefficient) between mitochondria and autophagosomes. Data represent the mean ± SEM of three independent experiments. ns = non-significant; * $P < 0.05$; ** $P < 0.01$; *** $P < 0.001$ (one-way ANOVA test).

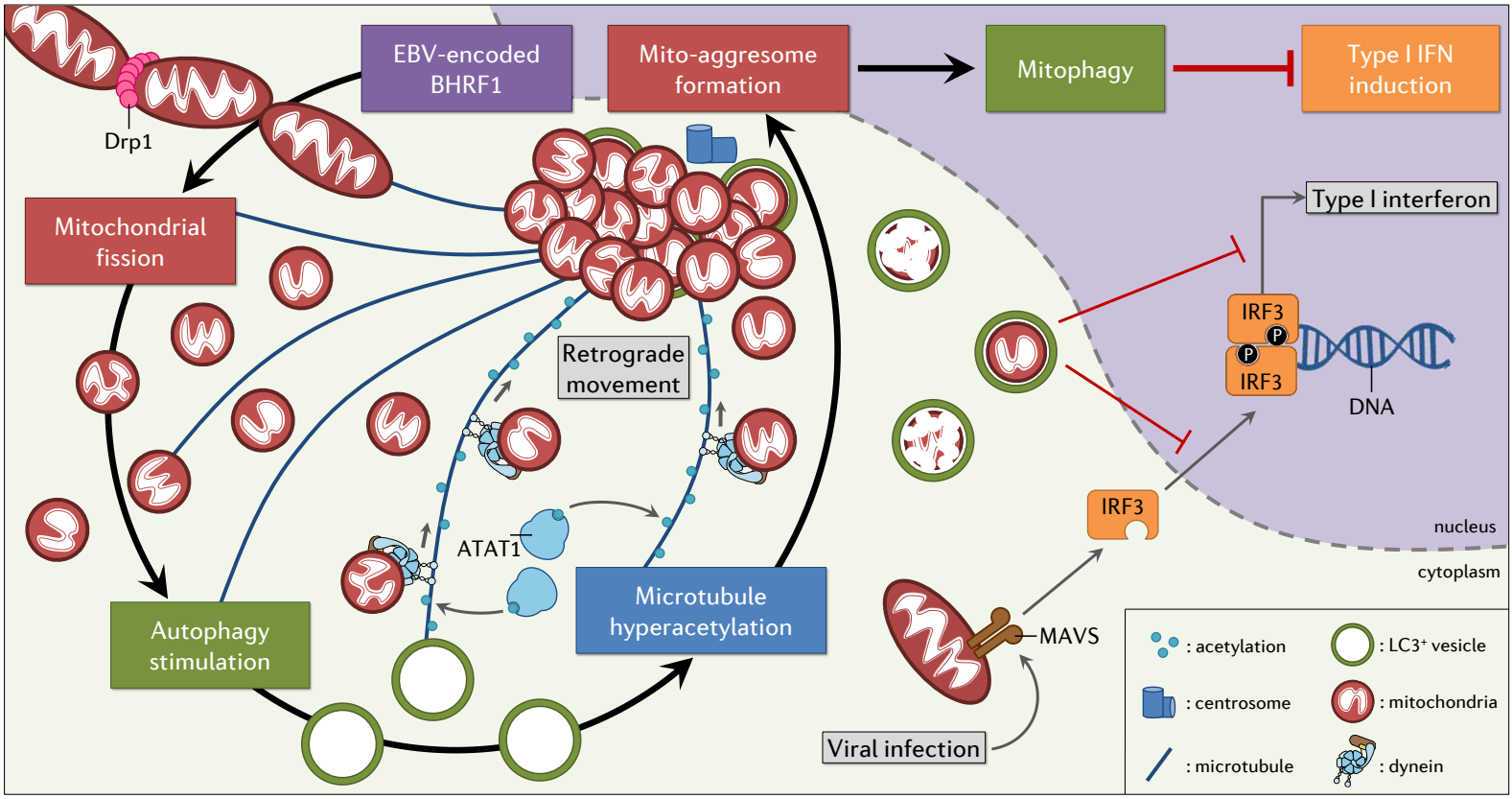

Figure 7. Working model. EBV encodes a Bcl-2 homolog that dampens type I IFN induction thanks to MT hyperacetylation. BHRF1 induces Drp1-mediated mitochondrial fission and subsequently autophagy. These cellular modifications lead to the mito-aggresome formation, and we showed here that the MT network and in particular its level of acetylation are essential for this mitochondrial phenotype. Moreover, BHRF1 induces MT hyperacetylation through ATAT1 activation. This hyperacetylation allows the retrograde transport of mitochondria in a dynein-dependent manner. Finally, the sequestration and degradation of mito-aggresomes block innate immunity.